Published online 20 November 2017

Nucleic Acids Research, 2018, Vol. 46, No. 1 ***293–313***
doi: 10.1093/nar/gkx1174

Translation can affect the antisense activity of RNase H1-dependent oligonucleotides targeting mRNAs

Xue-Hai Liang*, Joshua G. Nichols, Hong Sun and Stanley T. Crooke

Department of Core Antisense Research, Ionis Pharmaceutics, Inc., 2855 Gazelle Court, Carlsbad, CA 92010, USA

Received August 28, 2017; Revised November 03, 2017; Editorial Decision November 07, 2017; Accepted November 10, 2017

ABSTRACT

RNase H1-dependent antisense oligonucleotides (ASOs) can degrade complementary RNAs in both the nucleus and the cytoplasm. Since cytoplasmic mRNAs are actively engaged in translation, ASO activity may thus be affected by translating ribosomes that scan the mRNAs. Here we show that mRNAs associated with ribosomes can be cleaved using ASOs and that translation can alter ASO activity. Translation inhibition tends to increase ASO activity when targeting the coding regions of efficiently translated mRNAs, but not nuclear non-coding RNAs or less efficiently translated mRNAs. Increasing the level of RNase H1 protein eliminated the enhancing effects of translation inhibition on ASO activity, suggesting that RNase H1 recruitment to ASO/mRNA heteroduplexes is a rate limiting step and that translating ribosomes can inhibit RNase H1 recruitment. Consistently, ASO activity was not increased by translation inhibition when targeting the 3′ UTRs, independent of the translation efficiency of the mRNAs. Contrarily, the activity of 3′ UTR-targeting ASOs tended to be reduced upon translation inhibition, likely due to decreased accessibility. These results indicate that ASO activity can be affected by the translation process, and the findings also provide important information toward helping better ASO drug design.

INTRODUCTION

DNA-like antisense oligonucleotides (ASOs) are commonly used to down-regulate gene expression for both research and therapeutic purposes (1,2). ASOs are usually designed as chimeric gapmers composed of a central DNA portion, and flanked at both ends (wings) with RNA-like nucleotides. To enhance pharmacological and pharmacokinetic properties, currently used second generation, 5–10–5 gapmer ASOs are modified with 2′-*O*-methoxyethyl (MOE) at the wings, and each nucleotide is linked with phosphorothioate (PS) backbones (3,4). Upon base-pairing with target RNAs, ASOs can recruit RNase H1 to cleave the RNA substrate within the region complementary to the DNA portion of ASOs (5,6). RNase H1, which is expressed in cells at low levels and localizes in both the nucleus and the cytoplasm, is a limiting factor with regard to ASO-mediated antisense activity (7–10).

PS-ASOs can be delivered into cells either through transfection or by free uptake, i.e. incubation with cells without transfection reagents (11–15). ASOs are active both *in vitro* and *in vivo*, and can efficiently reduce the levels of both nuclear and cytoplasmic RNAs (9,10). Many factors are known to affect ASO activity, such as ASO uptake, intracellular distribution, protein binding, target RNA accessibility and stability, as well as the subcellular localization of the RNA (2,10,12,16–21). Nuclear localization of ASOs has been shown to positively correlate with ASO activity (22), and robust nuclear ASO activity has been well-documented (23,24). Recently, strong cytoplasmic activity of RNase H1-dependent ASOs has also been demonstrated (9,17), as evidenced by the observations that ASOs can reduced mRNA levels without obvious ASO nuclear localization upon free uptake (17), and that many ASOs can rapidly reduce cytoplasmic mature mRNAs without affecting the levels of nuclear pre-mRNAs, and rapid appearance of both 5′ and 3′ cleavage products in the cytoplasm upon transfection (9). However, the cellular processes that modulate ASO activity are still not fully understood, and it is uncertain why ASO activity varies in different cell types or tissues. Dissecting the mechanisms of action of ASOs is thus particularly important to further optimize the drug design, and to improve experimental design and interpretation.

Most mRNAs are transcribed in the nucleus as precursors, which are processed to generate mature mRNAs (25). Mature mRNAs are quickly exported to and enriched in the cytoplasm (26), where mRNAs are normally engaged in translation by the ribosomes. During translation, the 40S small subunit (SSU) together with initiator tRNA and translation initiation factors including the eIF4F complex, associates with the 5′ UTR of mRNAs either in a cap-dependent or in an Internal Ribosome Entry Site (IRES)-dependent manner, forming the pre-initiation complex (PIC) (27). PIC then scans the mRNA in a 5′-to-3′ direction, searching for the AUG start codon (28). Once the

*To whom correspondence should be addressed. Tel: +1 760 603 3816; Fax: +1 760 603 2600; Email: Lliang@ionisph.com

start codon is identified, the 60S large subunit (LSU) joins, forming the 80S ribosome which initiates translation (29). Within the mRNA coding region, the 80S ribosome continues to scan the open reading frame (ORF) during translation elongation. When the ribosome reaches a stop codon, release factors are recruited, translation stops, and 80S ribosome dissembles (30). The ribosome, equipped with unwinding activity, can melt mRNA structures to ensure the reading along the mRNA (31,32). A mRNA molecule can be translated simultaneously by more than one ribosome, forming poly-ribosomes (polysomes) (33,34).

Translation can be regulated either by *cis*-acting elements present in the mRNAs, e.g. 5′ UTR structures, the presences of upstream ORFs, and kozak consensus sequence, or by *trans*-acting elements such as protein binding (35–37). In addition, the 3′ UTR is also involved in translational regulation, via binding to different proteins such as PABP or miRNAs that can modulate translation or mRNA stability (38,39). The 5′ and 3′ termini of mRNA can be connected by protein–protein interactions between, for example, eIF4F complex and PABP protein (40). This interaction(s) leads to the formation of a closed loop of the mRNA, which plays a significant role in efficient translation probably by accelerating ribosome recycling (27,37). Different mRNAs can be translated with different efficiency, which is mainly determined by the rate limiting step, translation initiation (37). However, codon usage and mRNA structure have also been shown to affect the translation elongation rate (41). Efficiently translated mRNAs can be loaded with more 80S ribosomes per mRNA than the less efficiently translated mRNAs (42). Thus the average distance between two adjacent ribosomes on a mRNA is mainly determined by the initiation efficiency (43). In yeast, the average distance between two adjacent ribosomes was reported to be 154 nt (44). As translation occurs in eukaryotes at a rate of approximately 5.5–6 amino acids per second (45,46), and the median protein length is 375 aa in humans (47), it may take 1–2 min for a ribosome to complete the reading of a median length ORF. If a mRNA is translated simultaneously by multiple ribosomes, the time interval between two adjacent ribosomes on the same mRNA will be dramatically shortened.

RNase H1-dependent ASOs can trigger rapid degradation of mRNAs in the cytoplasm (9), where most mRNAs are translated under normal conditions. It is therefore possible that ASOs can act on translating mRNAs. In such cases, the activity of ASOs may be affected by the translating ribosomes, since the ASOs need to hybridize with mRNA targets, followed by the recruitment of RNase H1 protein for cleavage (10). Meanwhile, translating mRNAs are rapidly scanned by one or more ribosomes per mRNA, resulting in a limited time interval between two adjacent ribosomes (45,46,48), during which the ASO must bind, recruit RNase H1, and induce degradation of the mRNA. The scanning ribosomes may, in fact, remove ASOs from mRNA before the recruitment of RNase H1, leading to altered ASO activity. In short, ASO activity on mRNAs should be dependent on several rates: the On/Off rates of ASO binding, the rate of RNase H1 recruitment, the cleavage rate of RNase H1 and the rate of translation, to name a few.

To evaluate this hypothesis, here we analyzed the effects of translation on ASO activity using different approaches, and found that translation inhibition can increase the activity of ASOs when targeting the coding regions of efficiently translated mRNAs. Over-expression of RNase H1 abolished the enhancement of ASO activity by translation inhibition. However, translation inhibition tends to not increase the activity of ASOs targeting the less-efficiently translated mRNAs or nuclear non-coding RNAs or pre-mRNAs. No enhanced ASO activity was observed upon translation inhibition when targeting the 3′ UTRs, regardless of translation efficiency. Our results suggest that efficient translation tends to have negative effect on ASO activity when targeting the coding region sequences of mRNAs.

MATERIALS AND METHODS

ASOs, siRNAs and primer probe sets used in this study are listed in Supplementary Materials.

Cell culture, transfection, and drug treatment

HeLa, HEK293 and A431 cells were grown in DMEM medium, supplemented with 10% fetal calf serum (FCS) and 1% penicillin/streptomycin at 37°C in 5% or 8% CO_2 incubator. For ASO or siRNA transfection, cells were seeded at ∼50% confluence, incubated for ON, and transfected for 2.5 h with ASOs or siRNAs, using Lipofectamine 2000 or RNAiMax (Life Technologies). Cells were then treated with 100 μg/ml cycloheximide (CHX) (Sigma), 20 μM 4E1Rcat (Sigma), 20 μg/ml puromycin (ThermoFisher), or 625 nM lactimidomycin (LTM) (Millipore) for an additional 1.5 h, or mock treated with ethanol or DMSO, respectively. For specific translation inhibition of Nucleolin (*NCL*) mRNA, uniform PO/MOE ASOs were transfected at 40 nM into HeLa cells for 16 h, followed by transfection of gapmer ASOs for an additional 4h. Plasmid transfection was performed at 3 μg/15 cm dish using Lipofectamine 3000 (Life Technologies). For transduction, adenovirus expressing wild-type or catalytically inactive RNase H1 protein were added to HeLa cells at 15 MOI, incubated for 24 h, and split to 96-well plates. After incubation for an additional 18 h, ASOs were transfected for 2.5 h, followed by treatment with 100 μg/ml CHX for an additional 1.5 h. For ASO free uptake, A431 cells were incubated for ASOs without transfection for 16 h, followed by treatment with ethanol or 100 μg/ml CHX for an additional 1.5 h.

Luciferase activity assay

HeLa cells expressing a luciferase reporter (PXL52) as described in (49) were treated with 100 μg/ml CHX or 20 μM 4E1Rcat for 2 h. Cells were harvested and cell lysate was prepared using Glo Lysis Buffer (Promega). Firefly luciferase activity was measured using Dual-Glo Luciferase Assay system (Promega), and normalized to total protein levels quantified using Pierce BCA Protein Assay (ThermoFisher).

Sucrose gradient fractionation for polysome profiling

Polysome analyses were performed as described in (49). Briefly, ∼5 × 10^6 HeLa or HEK293 cells grown at ∼80%

confluency were treated for 15 min at 37°C with 100 μg/ml CHX. Cells were then washed with ice-cold 1 × PBS buffer containing 100 μg/ml CHX and harvested. Cell pellet was washed and resuspended in 800 μl lysis buffer (20 mM Tris pH 7.5, 5 mM $MgCl_2$, 100 mM KCl, 100 μg/ml CHX, 2 mM DTT, 1000 unit/ml of RNaseOut (ThermoFisher)). After incubation on ice for 10 min, cells were lysed by addition of 50 μl of 10% Triton X-100 and 50 μl of 10% sodium deoxycholate and incubated on ice for 5 min. Cell extracts were then cleared by centrifugation at 4°C for 5 min at 12 000 rpm, and 250 μl cell extract was loaded onto an 11 ml, 7–47% sucrose gradient. After centrifugation at 35 000 RPM for 2 h at 4°C using a SW41 rotor, fractions were taken from top to bottom at 400 μl each. RNA was prepared from each fraction using RNeasy (Qiagen), and rRNA or mRNAs were analyzed by quantitative real-time PCR (qRT-PCR).

For the analysis of ASO-mediated reduction of *NCL* mRNA in different ribosome fractions, HeLa cells were transfected or not transfected with *NCL* ASO110080 at 4 nM for 4h, treated with CHX, and harvested. Cell pellet was then resuspended in 800 μl lysis buffer supplemented with 300 pM of XL680 (∼3 fold of the transfected ASO110080), to inhibit post-lysis cleavage induced by the ASO. After fractionation, 10 μl aliquots from each fraction was pooled, and RNA was prepared to determine the *NCL* mRNA level after gradient fractionation. In addition, RNA was prepared from 200 μl of each fraction and analyzed by qRT-PCR as described below.

Immunoprecipitation

HeLa cells were transfected with a *Xrn1*-specific siRNA (5 nM) for 36 h, followed by transfection of the plasmid expressing GFP-RPL10a for 16 h. Next, cells were either mock-transfected or transfected with 40 nM ASO110080 for 4 h. Cells were then treated with 100 μg/ml CHX for 15 min at 37°C, washed 3 times using ice-cold 1 × PBS containing 100 μg/ml CHX, and collected. 1×10^7 Cells were resuspended in 800 μl lysis buffer supplemented with 3 nM XL680 to inhibit post-lysis cleavage. For mock-transfected cells, the buffer was also supplemented with 1 nM ASO110080 in addition to 3 nM XL680. Cell lysates were prepared as described above for polysome profile. 350 μl cell lysate was added to Protein A/G magnetic beads pre-coated with 15 μg anti-GFP antibody (TA50041, Origene) or mouse IgG, incubated at 4°C for 2 h, and washed five times with wash buffer (20 mM Tris pH 7.5, 5 mM $MgCl_2$, 150 mM KCl, 0.1% NP40, supplemented with RNaseOut). RNA was prepared using RNeasy column (Qiagen) from aliquots of washed beads. Co-isolated RNAs were analyzed by qRT-PCR, or were used for 5′ Rapid amplification of cDNA ends (5′ RACE). Aliquots of washed beads were loaded on SDS-PAGE, and proteins were determined by western blotting.

Detection of 5′ end of ASO-directed cleavage products by 5′ RACE

5′-RACE was performed using 5′/3′ RACE kit, second generation (Roche), based on the manufacturer's instructions. Briefly, cDNA was synthesized for immunoprecipitated RNA or total RNA prepared from input materials, with a *NCL* specific, antisense primer XL876 (5′-CGCTTTCTCCAGGTC TTCAG-3′). The cDNA was then purified using Pure PCR product Purification kit (Roche), and poly(A) was added to the cDNA using Terminal Transferase (Sigma). First step PCR was performed for 40 cycles (94°C, 30 s, 52°C 30 s, 68°C, 30 s) using the tailed cDNA as template, and a *NCL* specific primer XL877 (5′-AAAACATCGCTGATACC AGT-3′) and oligo dT-Anchor primer provided by the manufacturer. The PCR product was then used as templates for second step PCR performed for 40 cycles (94°C, 30 s, 52.5°C 30 s, 72°C, 30 s), using nested primers XL878 (5′-GAGATTGAAAGCCGTAGTCG-3′) and an anchor primer provided by the manufacturer. The PCR products were analyzed on a 2% agarose gel, cloned, and sequenced.

RNA preparation and qRT-PCR

Total RNA or RNA from sucrose gradient fractions was prepared using RNeasy (Qiagen), based on manufacturer's instructions. qRT-PCR was performed in triplicate using StepOne Real-Time PCR system and TaqMan primer probe sets as listed in Supplementary Materials, with AgPathID™ One-step RT-PCR kit (Applied Biosystems). qRT-PCR in 20 μl reactions was performed using the following program: 48°C for 10 min, 94°C for 10 min and 40 cycles of 20 seconds each at 94°C and 60°C. The qRT-PCR results were quantified using StepOne Software V2.3, calculated and plotted in Excel. Tested RNA levels in each reaction were normalized to total RNA levels measured using SYBR Green (Life Technologies), before being calculated for average values. For quantification of RNAs prepared from different gradient fractions, the relative RNA level in each fraction was calculated as percentage of the RNA in the fraction relative to the sum of the RNA levels in all fractions. Statistics was performed using Prism, with either *t*-test, or *F*-test for curve comparison based on non-linear regression (dose-response curves) for XY analyses, using equation 'log(agonist) vs normalized response – Variable slop'. The Y axis (relative level) was used as the normalized response.

In vivo RNA structural probing

HeLa cells grown at ∼80% confluence were treated at 37°C with 100 μg/ml CHX for 1.5 h, or with 20 μg/ml puromycin for 1.5 h followed by 100 μg/ml CHX treatment for 15 min. Dimethyl sulfate (DMS) treatment and RNA preparation was performed as previously described (49). 8 μg total RNA was used in primer extension reaction using 5′-end ^{32}P-labeled primer XL877 or XL845 for different regions of *NCL* mRNA. The extension products were analyzed on an 8%, 7M urea PAGE gel, and the results were visualized by autoradiography.

Western analyses

Cells were collected using trypsin and washed with 1 × PBS. Cell lysate was prepared using RIPA buffer (ThermoFisher) and cleared by centrifugation at 10 000 × g

for 10 min at 4°C. Proteins (20–40 μg/lane) were separated by 4–12% SDS-PAGE, transferred to membrane, and specific proteins were detected with specific antibodies, and visualized using ECL. The following antibodies were purchased from Abcam: La (ab75927), NPM1 (ab24412), Ku70 (ab3114), TCP1β (ab92746), PC4 (ab72132), ANXA2 (ab54771), NCL (ab13541), AGO_2 (Ab57113), RPL10a (ab174318) and DDX6 (ab40684). P54nrb (sc-376865) and Xrn1 (sc-165984) antibodies were purchased from Santa Cruz Biotechnologies. Anti-GFP antibodies (TA50041 for IP and TA150096 for western) were from Origene. A rabbit RNase H1 antibody was kindly provided by Hongjiang Wu (Ionis Pharmaceuticals). Anti-rabbit secondary antibody conjugated to HRP (170-6515) and anti-mouse secondary antibody conjugated to HRP (170-6516) were purchased from Bio-Rad.

Immunofluorescent staining

HeLa cells were transfected with 40 nM Cy3-labeled ASO 446654 for 2.5 h, and treated or nor treated with 100 μg/ml CHX for an additional 1.5 h. Cells were then washed with PBS, fixed with 4% paraformaldehyde for 30 min, and images were taken using confocal microscope (Olympus FV-1000) and processed using FV-10 ASW 3.0 Viewer (Olympus). For P-body staining, HeLa cells treated with control or 100 μg/ml CHX, or 20 μM 4E1Rcat for 2 h were washed with 1 × PBS, fixed with 4% paraformaldehyde for 30 min at room temperature, and permeabilized for 5 min with 0.1% Triton in PBS. After blocking at room temperature for 30 min with block buffer (1 mg/ml BSA in 1 × PBS), cells were incubated for 2 h with anti-DDX6 antibody in block buffer, washed three times (5 min each) using wash buffer (0.1% NP-40 in 1 × PBS), and incubated for 1 h with anti-Rabbit secondary antibody conjugated with AF488 (Abcam, ab150077, 1:200). After washing three times, cells were mounted with Anti-fade reagent containing DAPI (Life Technologies), and images were taken and processed using the confocal microscope as described above.

RESULTS

Translation inhibition can affect ASO activity in reducing target mRNA levels

HeLa cells were transfected with RNase H1-dependent, 5–10–5 gapmer ASOs targeting either *Nucleolin* (*NCL*) or *PTEN* mRNA. As a control, an ASO targeting a nuclear retained non-coding RNA, Malat1, was also tested. These target RNAs were chosen as they have been well studied in our previous efforts to evaluate ASO activities (18,19). ASOs were transfected for 2.5 h to ensure sufficient delivery, and then translation was inhibited for an additional 1.5 h by cycloheximide (CHX), a commonly used antibiotic that inhibits translation elongation (50). As many tested ASOs can reach maximum activity within 4 h after transfection (9), and protein half-lives are relatively long (e.g. the average protein turnover rate in HeLa cells was reported to be 20 h (51)), the experimental conditions used here should allow us to determine the effects of translation inhibition on ASO activity without substantial effects of CHX on global protein levels.

qRT-PCR quantification results showed that, upon CHX treatment, the activity of the *NCL*-targeting ASO was dramatically increased as compared with ethanol control treatment, as evidenced by the greater mRNA reduction (Figure 1A). The IC_{50} was reduced from ∼3.52 to 0.48 nM upon CHX treatment. Interestingly, the activity of the ASO targeting *PTEN* mRNA was not increased (Figure 1B). As a control, the ASO targeting the untranslated Malat1 RNA showed comparable activity with or without CHX treatment (Figure 1C). The effectiveness of CHX on translation was confirmed by the observation of reduced luciferase activity in *Firefly* luciferase-expressing HeLa cells with similar CHX treatment (Figure 1D). Luciferase is known to be short-lived, with a half-life less than 3h (52). These experiments (and subsequent experiments) were performed more than three times and similar observations were obtained (data not shown).

Enhanced activity of the *NCL* ASO by CHX treatment was also observed in human A431 cells when ASOs were delivered by free uptake (Supplementary Figure S1A). The IC_{50} was reduced from 3.73 to 0.35 μM by CHX treatment. Consistent with the observations using transfection in HeLa cells, the activities of ASOs targeting *PTEN* mRNA and Malat1 RNA were not enhanced by CHX treatment upon free uptake (Supplementary Figure S1B and C), indicating that the observed effects are not unique to transfection or unique to HeLa cells. Indeed, enhanced activity by CHX treatment was observed for the *NCL* ASO (Supplementary Figure S1D), but not for the *PTEN* and Malat1 ASOs (Supplementary Figure S1E and F), in HEK293 cells upon transfection.

The CHX effect on the *NCL* ASO activity is unlikely to have resulted from unexpected global effects caused by the drug, as under the same conditions, the ASO activities targeting *PTEN* and Malat1 RNAs were not enhanced. The RNA levels of *NCL* and Malat1 were not substantially altered by CHX treatment under these experimental conditions (Supplementary Figure S2A), although a slight increase was observed for *PTEN* mRNA, consistent with previous reports that CHX can stabilize some mRNAs (53). These results indicate that the increased activity of the *NCL* ASO was not due to altered mRNA basal levels. In addition, transfection efficiency and subcellular distribution of the ASOs appeared comparable in control and CHX treated cells (Supplementary Figure S2B). Moreover, although some proteins are known to affect ASO activity, such as RNase H1, La/SSB, NPM1, Ku70, TCP1β, PC4, P54nrb and ANXA2 (13,18,19,54), the levels of these proteins were not substantially affected by CHX treatment for this short time (Supplementary Figure S2C).

Other translation inhibitors caused similar effects on the ASO activities

To further determine if the enhanced *NCL* ASO activity was caused by translation inhibition and not by an unexpected effect of CHX, HeLa cells were transfected for 2.5 h with ASOs, and subsequently treated for 1.5 h with 4E1Rcat, a small molecule that inhibits cap-dependent translation initiation by disrupting the interaction between eIF4E and eIF4G proteins (55). Upon 4E1Rcat treatment, the activ-

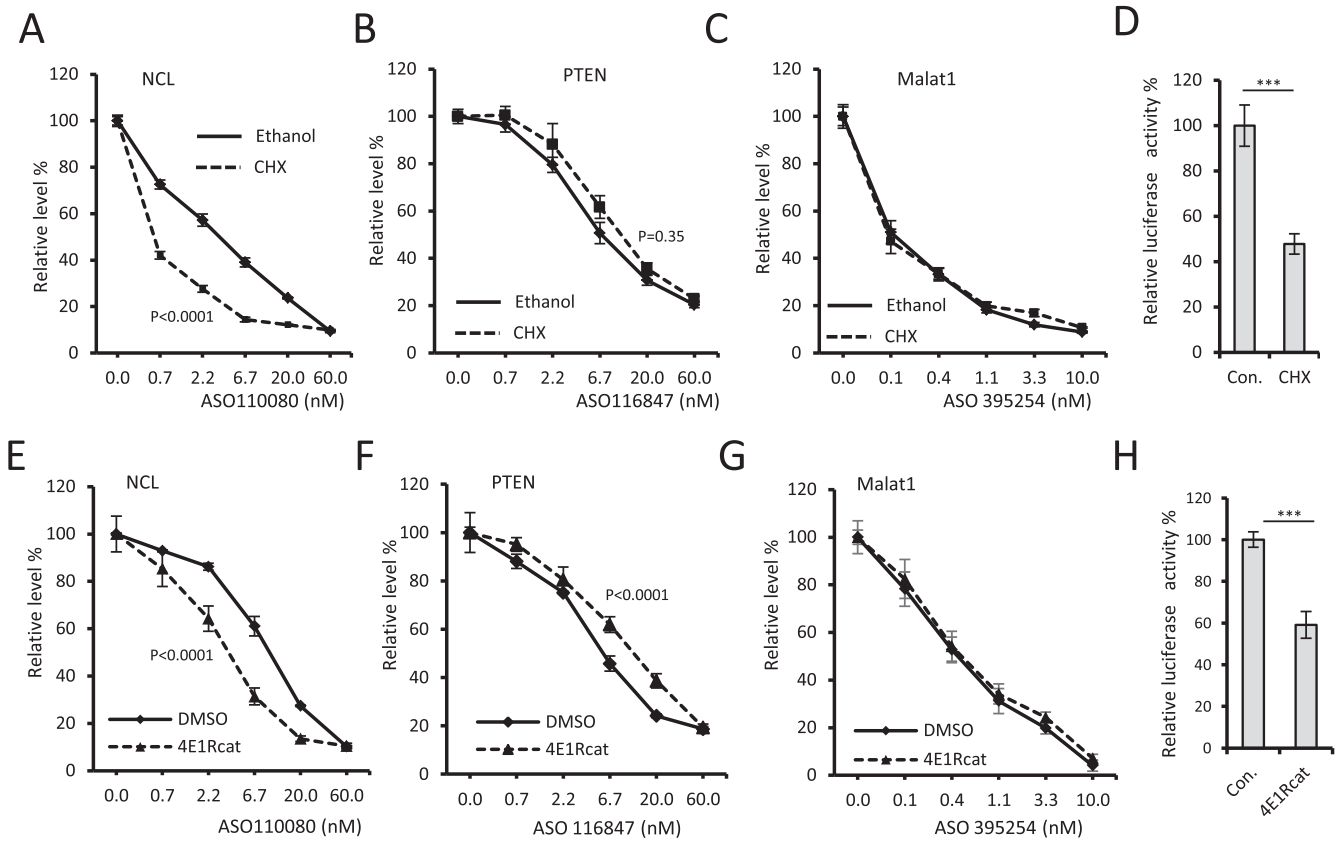

Figure 1. CHX treatment can enhance the activity of the ASO targeting *NCL* mRNA. HeLa cells were transfected for 2.5 h with ASOs targeting *NCL* mRNA (**A**), *PTEN* mRNA (**B**) or Malat1 RNA (**C**) at different final concentrations, followed by treatment with 100 μg/ml CHX or ethanol for an additional 1.5 h. The levels of targeted RNAs were quantified by qRT-PCR and plotted. (**D**) Luciferase activity assay for HeLa cells transiently expressing the *Firefly* luciferase treated with 100 μg/ml CHX or ethanol (Con.) for 2 h. (**E–G**) qRT-PCR quantification of *NCL* mRNA (E), *PTEN* mRNA (F), or Malat1 RNA (G) in HeLa cells transfected with the corresponding ASOs for 2.5 h, followed by treatment with 20 μM 4E1Rcat or DMSO control for an additional 1.5 h. (**H**) Luciferase activity assay for HeLa cells transiently expressing the firefly luciferase treated with 20 μM 4E1Rcat or DMSO (Con.) for 2 h. X-axis represents ASO concentration in nM (unscaled). '0' indicates mock transfection. The error bars in each panel are standard deviation from three independent experiments. *P*-values were calculated using t-test (panels D, H) or *F*-test based on non-linear regression (curve fit) using Prism.

ity of the *NCL* ASO was again enhanced (IC_{50} was reduced from 10.02 to 4.2 nM) (Figure 1E), whereas the activity of the *PTEN* ASO was slightly reduced (Figure 1F), and no activity change was observed for the Malat1 ASO (Figure 1G), as compared with DMSO treated control cells. The effectiveness of 4E1Rcat on translation was confirmed by the reduced luciferase activity upon treatment (Figure 1H). Similar effects of translation inhibition on ASO activity were also observed using puromycin (Supplementary Figure S3A), which causes pre-mature peptide release and dissociation of ribosome subunits (56), or using lactimidomycin (LTM) (Supplementary Figure S3B), which inhibits translation initiation (50). Together, these results suggest that the enhanced activity for the *NCL* ASO was not unique to CHX treatment, and most likely it was caused by translation inhibition. In alignment with the fact that translation occurs in the cytoplasm where mRNAs are enriched, the ASO reduced mature *NCL* mRNA levels after 4h treatment (Figure 1A), but not the level of *NCL* pre-mRNA (Supplementary Figure S4A), suggesting an early and direct cytoplasmic cleavage of the mature mRNA by the ASO treatment, in agreement with our previous findings (9).

Although CHX treatment did not substantially change the level of mature *NCL* mRNA, the level of *NCL* pre-mRNA was decreased (Supplementary Figure S4B), consistent with previous reports that CHX treatment can reduce pre-mRNA levels (50,57). However, the enhanced activity of the *NCL* ASO was unlikely caused by the decreased pre-mRNA level, as 4E1Rcat treatment did not alter the levels of *NCL* pre-mRNA and mature mRNA (Supplementary Figure S4C), but still increased the activity of the *NCL* ASO. Moreover, inhibition of transcription for 2 h using 5,6-dichloro-1-beta-D-ribofuranosylbenzimidazole (DRB) dramatically decreased the level of *NCL* pre-mRNA (Supplementary Figure S4D), however, DRB treatment did not alter the activity of the *NCL* ASO (Supplementary Figure S4E). In addition, although CHX treatment reduced the formation of P-bodies (Supplementary Figure S5A and B), consistent with previous studies (58), 4E1Rcat treatment did not, suggesting that the enhanced *NCL* ASO activity by the two drugs was not a consequence of altered formation of P-body, which may contain some translation-arrested mRNAs and enzymes required for mRNA degradation (59). Altogether, these results suggest that transla-

tion inhibition led to the enhanced activity of the ASO targeting *NCL* mRNA.

NCL mRNA is more efficiently translated than *PTEN* mRNA

The different effects of CHX (and other translation inhibitors) on the activities of ASOs targeting *NCL*, *PTEN* mRNAs and Malat1 RNA are interesting. Malat1 is a nuclear localized lncRNA, thus we expected that translation inhibition should have no effect on the activity of the Malat1 ASO, and indeed, this was observed. Consistently, CHX treatment also did not affect the activity of two ASOs in reducing *AGO2* pre-mRNA in the nucleus (Supplementary Figure S6). These ASOs were found previously to be active in degrading *AGO2* pre-mRNA (9). However, both *NCL* and *PTEN* mRNAs are translated, yet only *NCL* ASO activity was enhanced by translation inhibition. It is thus possible that these two mRNAs may differ in other ways, such as translation efficiency.

To evaluate this possibility, polysome profiles were analyzed using sucrose gradient fractionation, followed by qRT-PCR for the levels of *NCL* and *PTEN* mRNAs. The results showed that *NCL* mRNA was enriched mainly in the heavy polysome fractions (more ribosomes per mRNA) toward the bottom of the gradient (Figure 2A), whereas *PTEN* mRNA was enriched in the 80S monosome and light polysome regions (fewer ribosomes per mRNA) (Figure 2B), as shown by the migration pattern of 28S rRNA, which marks the positions of 80S and polysomes (Figure 2C). These results indicate that more ribosomes were loaded to each *NCL* mRNA than to *PTEN* mRNA, and that *NCL* mRNA is more efficiently translated than the *PTEN* mRNA in cells.

ASOs can trigger cleavage of the *NCL* mRNA associated with ribosomes

The higher translation efficiency of *NCL* mRNA than *PTEN* mRNA may explain the enhanced activity caused by translation inhibition for the *NCL* ASO, but not for the *PTEN* ASO, as the *NCL* ASO may be affected by the relatively short time interval between two adjacent ribosomes when targeting the translating mRNAs. If this is the case, the ASOs should be able to act on translating mRNAs and reduce the levels of mRNAs in mono-ribosome and polysome fractions. To evaluate this hypothesis, we transfected HeLa cells for 4h with the *NCL* ASO, at 4 nM concentration (approximate IC_{50}, Figure 1A), to better determine if reduction of mRNAs occurs during translation and if so, in which ribosome fractions degradation of the mRNA may happen. To inhibit post-lysis cleavage induced by the transfected ASO, cell lysate was prepared in the presence of excess amount of a 2′-*O*-methylated oligoribonucleotide (XL680) complementary to the *NCL* ASO. As expected, no further *NCL* mRNA reduction was observed after gradient fractionation, as determined by qRT-PCR in total RNA samples prepared from cell lysates or from pooled gradient fractions after fractionation (Figure 3A).

Sucrose gradient fractionation was then performed using cell lysates prepared from mock transfected cells or cells

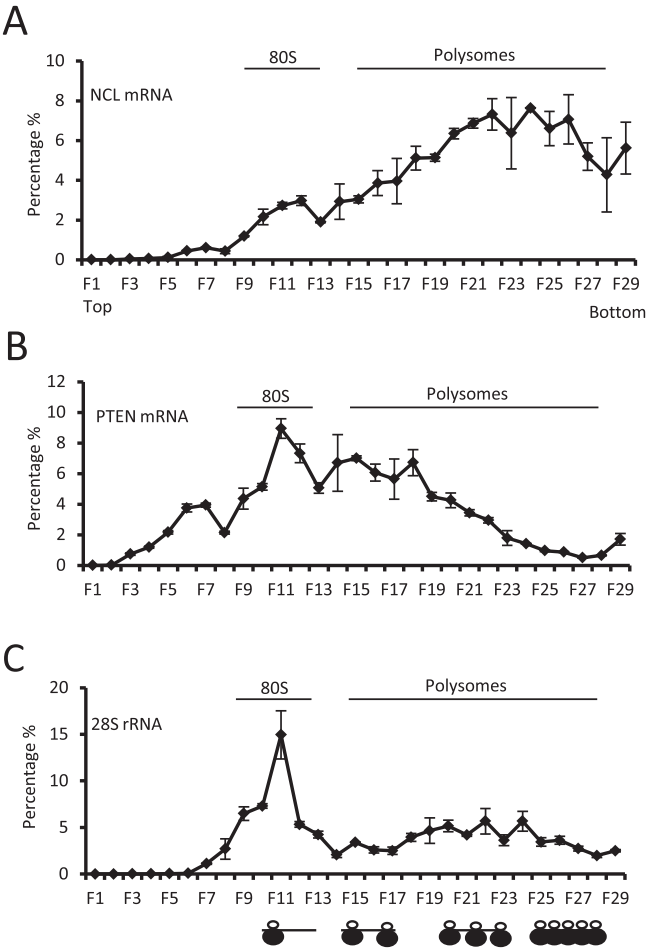

Figure 2. *NCL* mRNA migrates in heavy polysome fractions. Sucrose gradient fractionation was performed as described in Materials and Methods. RNA was prepared from each fraction and subjected to qRT-PCR analyses for the levels of *NCL* mRNA (**A**), *PTEN* mRNA (**B**) and 28S rRNA (**C**). The percentages of the RNAs in each fraction relative to the sum of all fractions were calculated and plotted. The error bars represent standard deviation of three experiments. The 80S and polysome regions are indicated based on the migration of the 28S rRNA. A schematic depiction for mono-ribosome and polysomes is shown below panel C.

treated for 4 h with the *NCL* ASO. qRT-PCR results showed that the levels of *NCL* mRNA were similarly reduced in both 80S mono-ribosome and polysome fractions by the ASO treatment, as compared with mock transfection (Figure 3B). As a control, the levels and migration patterns of 28S rRNA were not affected by the ASO transfection (Figure 3C). These results support the possibility that the ASO can induce cleavage of *NCL* mRNAs associated with ribosomes.

To determine if ASO-mediated cleavage can indeed occur on translating mRNAs, we sought to co-immunoprecipitate cleaved mRNA fragments associated with ribosomes. To inhibit rapid degradation of the cleaved products, the 5′→3′ exonuclease Xrn1 was reduced by siRNA treatment (Supplementary Figure S7A-B), as this protein is involved in the degradation of the 3′ cleaved fragments (60). To immunoprecipitate the ribosomes, a GFP-tagged RPL10a protein was transiently expressed in the Xrn1 reduced cells (Sup-

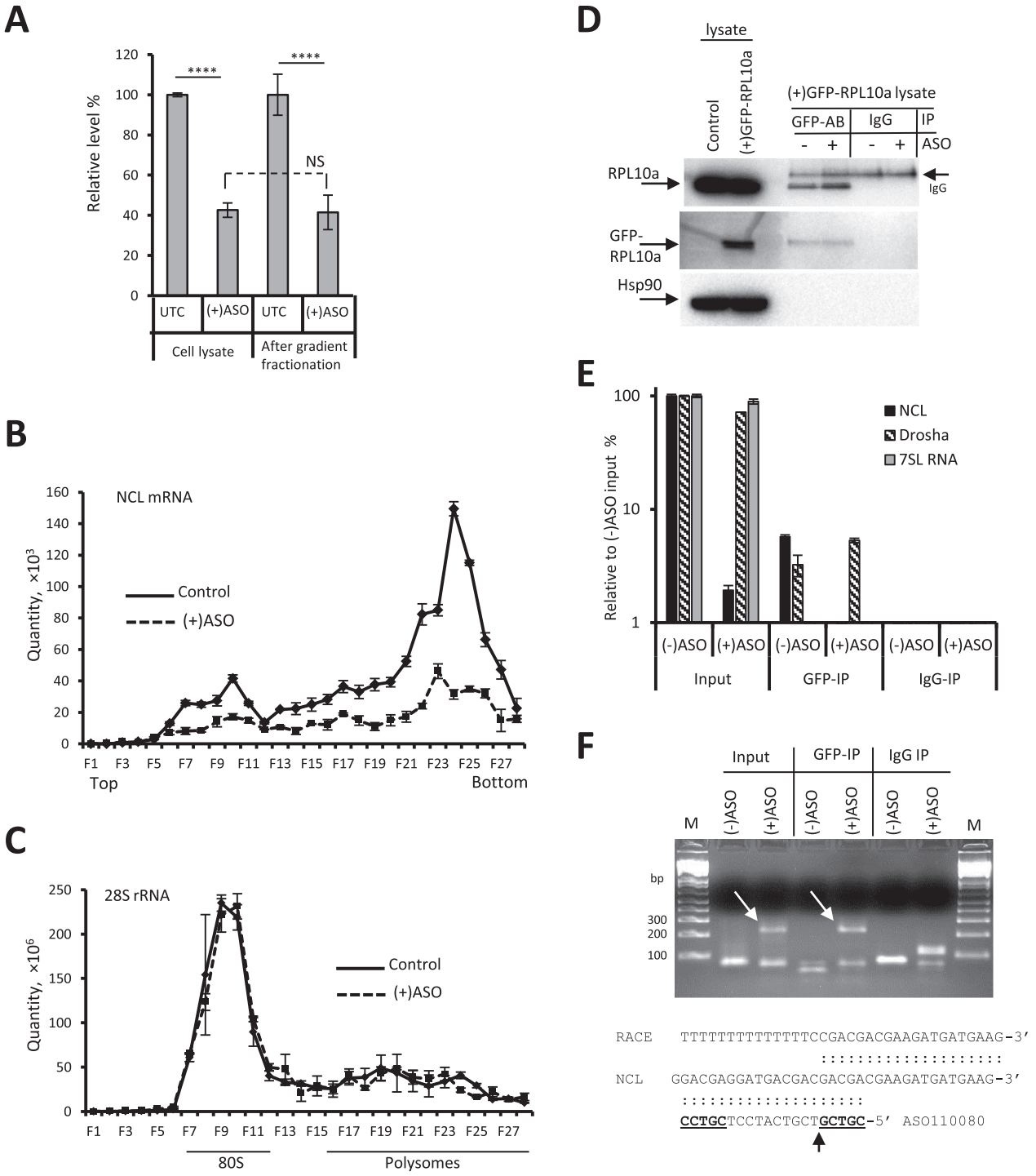

Figure 3. *NCL* mRNA associated with ribosome can be degraded by ASO transfection. (**A**) qRT-PCR quantification of *NCL* mRNA levels in total cell lysates and in pooled samples from each sucrose gradient fractions, as described in Materials and Methods. UTC, mock treated control. (**B**) qRT-PCR quantification of *NCL* mRNA in different sucrose gradient fractions for cell lysates prepared from mock-treated control cells or *NCL* ASO transfected cells ((+)ASO). The *NCL* mRNA quantity in unit was calculated for control and ASO-transfected cells using RNA standards in qRT-PCR assay. (**C**) qRT-PCR quantification of 28S rRNA in different fractions, as in panel B. the error bars represent standard deviation of three experiments. *P*-values were calculated based on *t*-test. (**D**) Western analyses for proteins co-isolated with anti-GFP antibody. The blot was probed with anti-RPL10a antibody (upper panel) or anti-GFP antibody (middle panel). Hsp90 was detected and served as a control. The IgG band from the boiled beads was detected by the RPL10a antibody and is indicated. IP, immunoprecipitation. (**E**) qRT-PCR quantification of *NCL* and *Drosha* mRNAs and 7SL RNA. In input samples, the RNA levels were normalized to total RNA measured using SYBR-Green, and calculated relative to the same RNA level in the (–)ASO sample. For the precipitated samples, the RNA levels were calculated relative to the same RNA level in the input material from (–)ASO samples. Error bars represent standard deviation from three independent experiments. (**F**) Agarose gel separation of the PCR products of 5′RACE. The RACE products are marked with arrows. M, DNA ladder (1 kb Plus, Life Technologies). The PCR product was cloned and sequenced. The sequencing result is shown at the lower panel. The arrow indicates the detected 5′-end of the 5′RACE product. The underlined nucleotides in the ASO sequence indicate the 2′-*O*-MOE modified wing regions.

plementary Figure S7C). This N-terminal GFP-targeted RPL10a protein has been shown to be functional and is commonly used for co-isolation of ribosome/polysome-associated RNAs (61,62). Next, ASO110080 was transfected into the GFP-RPL10a expressing cells for 4 h, and cell lysate was prepared in the presence of excess amounts of the complementary oligonucleotide XL680 to inhibit post-lysis cleavage. As a control, lysates were also prepared from mock-transfected cells, but the ASO110080 was added to the lysis buffer, along with the XL680 oligonucleotides. Immunoprecipitation was performed using an anti-GFP antibody, which co-isolated both the GFP-tagged and wild-type RPL10a proteins, as determined by western analyses (Figure 3D). Co-precipitation of the wild-type RPL10a is most likely due to the co-isolation of polysomes linked by mRNAs. The GFP-RPL10a or RPL10a was not detected in the IgG precipitated samples. As a control, the abundant Hsp90 protein was not co-isolated with either IgG or anti-GFP antibody.

To further determine the specificity of the immunoprecipitation, co-isolated RNAs were analyzed by qRT-PCR (Figure 3E). As expected, *NCL* mRNA was co-isolated with the anti-GFP antibody from mock-transfected cells, but not substantially from the ASO-transfected cells, in which the *NCL* mRNA was dramatically reduced, as seen from the input samples. As a control, the un-targeted *Drosha* mRNA was comparably co-isolated with GFP-RPL10a from both ASO transfected and untransfected cells. A ncRNA, 7SL RNA, was not substantially co-isolated, suggesting no- or little contamination. None of the three RNAs was meaningfully co-precipitated with the IgG control.

The co-isolated RNAs were then analyzed by 5′ RACE to detect the cleavage product of *NCL* mRNA induced by the ASO. Only from ASO-transfected cells was a RACE PCR product detected at expected size from the input sample, and importantly, also from the GFP-RPL10a precipitated sample (Figure 3F, upper panel). Without ASO transfection, no RACE product was detected from either input or precipitated samples, suggesting that the detected RACE product was not derived from post-lysis cleavage. The 5′-end of the RACE product was determined by sequencing, and was found to localize in a region that base-pairs with the DNA portion of the 5–10-5 gapmer ASO (Figure 3F, lower panel), consistent with the characteristic of RNase H1-mediated cleavage. Note that the 5′ end was adjacent to the 5′ MOE wing of the ASO, likely due to incomplete depletion of Xrn1 protein, which might still cause some exonucleolytic trimming of the cleavage product. Nonetheless, these results indicate that transfected ASOs can trigger the cleavage of ribosome-associated mRNA, which is most likely being translated.

Over-expression of RNase H1 attenuated the enhancement in ASO activity by CHX treatment

As described above, it is possible that the time interval between two adjacent ribosomes on the efficiently translated *NCL* mRNA is limited, which may affect the ASO binding and/or RNase H1 recruitment under normal conditions. If the enhanced activity of the *NCL* ASO by translation inhibition was due to ribosome arrest that provided sufficient time for ASO hybridization and RNase H1 recruitment, over-expression of RNase H1 should reduce the effect of CHX on the ASO activity, since higher level of RNase H1 protein may increase the rate of recruitment. To evaluate this possibility, HeLa cells were transduced with adenoviruses expressing either the wild-type RNase H1, or a catalytically inactive mutant (7). Both the wild-type and mutant RNase H1 proteins were expressed at a level more than 8-fold higher than the endogenous protein (Figure 4A).

Next, control cells or cells over-expressing the RNase H1 proteins were transfected with ASOs, followed by CHX treatment. The activity of the *NCL* ASO110080 was once again increased upon CHX treatment in mock-treated cells (Figure 4B). Over-expression of the mutant RNase H1 altered neither the ASO activity nor CHX effects, as compared with that in control cells. As expected, over-expression of wild-type RNase H1 increased the ASO activity (red solid line), however, CHX treatment did not further increase the ASO activity in these cells (red dashed line). Similar effects were also observed for an ASO targeting *La* mRNA (Figure 4C), which showed enhanced activity upon CHX treatment in control cells (and see below), but not further enhanced by CHX treatment in cells over-expressing the wild-type RNase H1. Although the activity of the *PTEN* ASO was increased in cells over-expressing the wild-type RNase H1, but not the mutant, CHX treatment reduced the activity of this ASO in cells over-expressing the wild-type protein (Figure 4D), suggesting that the activity of the *PTEN* ASO was not limited by the level of RNase H1 protein. Together, these results indicate that CHX effect on ASO activity can be altered by the level of functional RNase H1 protein, and suggest that recruitment of RNase H1 is rate limiting and the short interval of translation of the efficiently translated *NCL* (and *La*, see below) mRNA, but not the less-efficiently translated *PTEN* mRNA, is sufficient to reduce the efficiency of RNase H1 recruitment (see discussion).

Specific inhibition of *NCL* mRNA translation enhanced the activity of the *NCL*-targeting ASO

Since CHX and other tested inhibitors can inhibit global translation, such treatment may cause unexpected effects that contribute to the altered activity of the *NCL* ASO. To exclude this possibility and to confirm that the increased ASO activity resulted from translation inhibition of the target mRNA, we sought to specifically inhibit translation of *NCL* mRNA using an oligonucleotide complementary to its 5′ UTR, at a position adjacent to the 5′ cap, as it has been shown that stem structures of 5′ UTR can inhibit translation when close to the cap (63). This oligonucleotide is uniformly modified with 2′-*O*-MOE, a form that does not trigger RNase H1 cleavage but can serve as a steric blocker to inhibit translation of the targeted mRNA in a position dependent manner (49,64). As a control, a uniformly modified oligonucleotide was designed to base-pair with the 5′ UTR of a different mRNA, the *NPM1* mRNA.

Upon transfection, the *NCL* blocker oligonucleotide, but not the control *NPM1* oligonucleotide, shifted *NCL* mRNA toward the top of the gradient, as compared with mock-transfected control cells (Figure 5A). We note that the

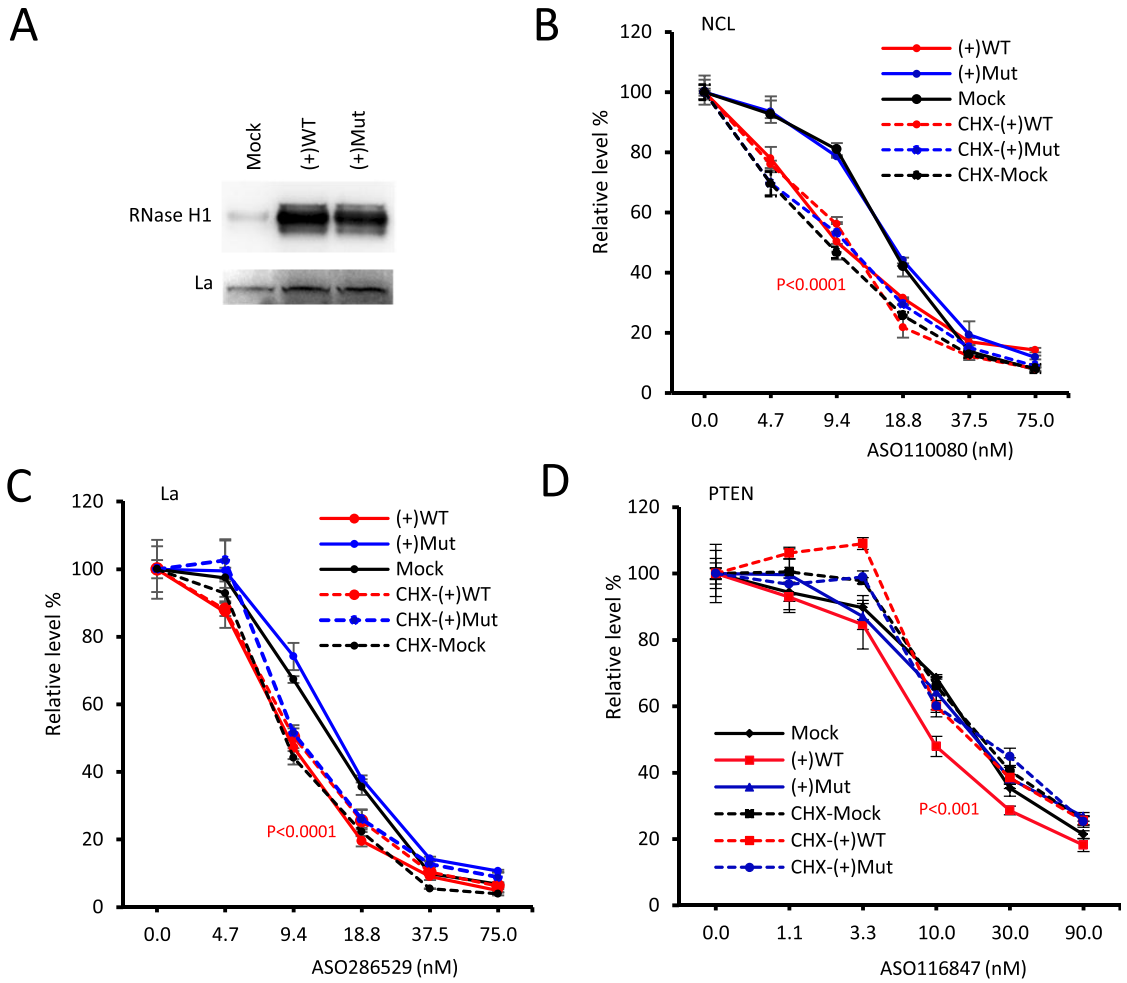

Figure 4. Over-expression of RNase H1 abolished the enhancement effects of CHX on the activity of the *NCL* ASO. (**A**) Western analysis for RNase H1 protein in mock treated HeLa cells and in cells transduced with adenovirus expressing wild-type ((+)WT) or a catalytically inactive mutant RNase H1 protein ((+)Mut). La protein was detected and served as a control for loading. (**B**) qRT-PCR quantification of *NCL* mRNA levels in different test cells transfected with ASO110080 for 2.5h, followed by treatment with (dashed lines) or without (solid lines) CHX for another 1.5 h. (**C**) qRT-PCR quantification of *La* mRNA in different test cells treated with ASO286529, as in panel B. (**D**) qRT-PCR quantification of *PTEN* mRNA in test cells treated with ASO116847. The error bars represent standard deviation of three experiments. *P*-values were calculated for difference between mock treated control cells (Mock) and cells over-expressing the wild type RNase H1 ((+)WT) in the absence of CHX, using F-test based on non-linear regression (curve fit) using Prism.

cell confluency (∼90%) was comparable across the three test cells in this experiment, but was higher than those used in other experiments (∼50–70% cell confluency). This may explain the observation that *NCL* mRNA, though still heavily enriched in polysomes, was shifted from heavy polysomes toward lighter polysomes as compared with that in Figure 3, likely due to reduced translation in confluent cells (65). Nevertheless, the results clearly showed that the *NCL* blocker reduced translation of *NCL* mRNA. As expected, the level of *NCL* mRNA was not reduced by the blocker oligonucleotide treatment (data not shown) (49).

The polysome profile of the *NPM1* mRNA appeared comparable in cells treated with either *NCL* or *NPM1* blocker, with no substantial shift when compared with mock transfected cells (Figure 5B). These results suggest that translation of *NCL* mRNA was specifically reduced by the *NCL* blocker, but not by the *NMP1* targeting oligonucleotide, which was also not inhibitory for *NPM1* translation. This is not surprising, since many oligonucleotides may not be active in targeting RNAs in cells, due to various reasons including inaccessibility of the target sites. This was further confirmed by western analysis, which showed that NCL protein was reduced by the *NCL* blocker, but not by the oligonucleotide targeting *NPM1*, and that NPM1 protein was not reduced by either oligonucleotide (Figure 5C), consistent with the polysome profiles.

Next, we evaluated the effects of specific inhibition of *NCL* mRNA translation on RNase H1-dependent ASO activity. HeLa cells were first transfected with the *NCL* or *NPM1* blocker oligonucleotides for 16 h to specifically inhibit *NCL* mRNA translation, and gapmer ASOs targeting *NCL*, *PTEN* or *NPM1* mRNAs were subsequently transfected for 4 h. Again, enhanced activity for the *NCL* ASO was observed in cells specifically inhibited of *NCL* translation, as compared with cells treated with the control *NPM1* blocker oligonucleotide (Figure 5D). The activities of the

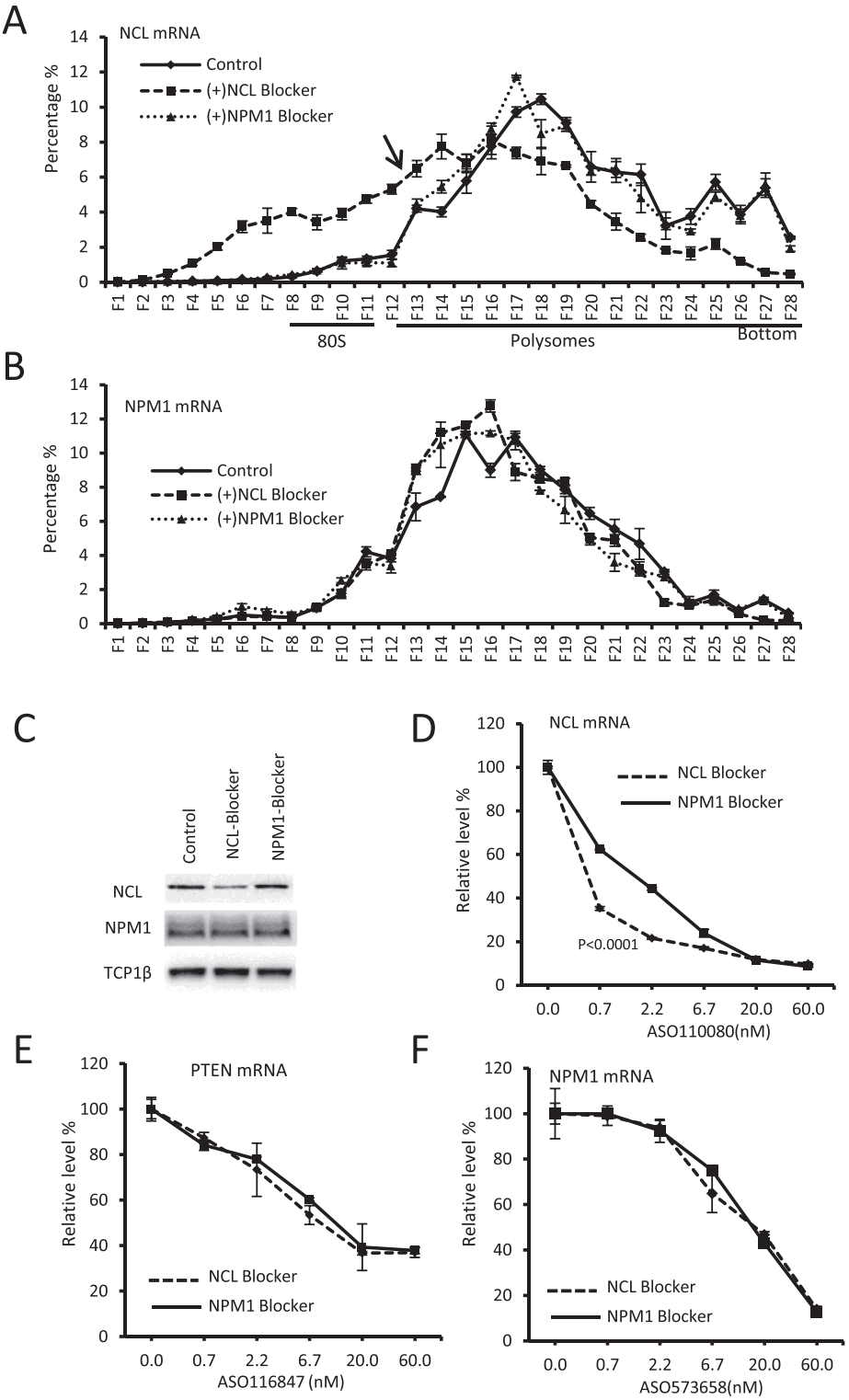

Figure 5. Specific inhibition of *NCL* mRNA translation enhanced the *NCL* ASO activity. (**A**) HeLa cells were either mock transfected (control), or transfected for 16 h with 40 nM uniform blocker oligonucleotides targeting either *NCL* or *NPM1* mRNA. Sucrose gradient fractionation was performed as described in Materials and Methods. *NCL* mRNA levels in different fractions were determined by qRT-PCR. The 80S and polysome fractions were determined by the migration of 28S rRNA (not shown). The shifted *NCL* mRNA toward the top of the gradient is marked with an arrow. (**B**) qRT-PCR quantification of *NPM1* mRNA in the same gradient fractions as in panel A. (**C**) Western analyses for the levels of NCL and NPM1 proteins in HeLa cells treated with the blocker oligonucleotides for 16 h. TCP1β was detected and served as a control for loading. (D–F) qRT-PCR quantification of *NCL* mRNA (**D**), *PTEN* mRNA (**E**), or *NPM1* mRNA (**F**) in HeLa cells transfected with the blocker ASOs for 16 h, followed by transfection of the corresponding RNase H1-dependent gapmer ASOs for 4 h. The error bars represent standard deviation of three experiments. *P*-values were calculated using *F*-test based on non-linear regression (curve fit) using Prism.

ASOs targeting *PTEN* or *NPM1* mRNAs were comparable in the two test cells (Figure 5E and F), suggesting that the altered *NCL* ASO activity was specific to the blocker oligonucleotide and not caused by pre-transfection. Together, these results indicate that translation inhibition, and not unexpected effects of the inhibitors, resulted in the enhanced activity of the ASO110080 targeting *NCL* mRNA.

Translation inhibition can enhance the activity of other ASOs targeting *NCL* mRNA

ASO110080 targets a coding region sequence of *NCL* mRNA. To determine whether the observed effects of translation inhibition on ASO activity apply to other ASOs targeting *NCL* mRNA, 80 PS/MOE gapmer ASOs were synthesized that base-pair with different regions of the *NCL* mRNA, including 5′ UTR, coding region, and 3′ UTR (Figure 6A). These ASOs were transfected into HeLa cells at 15 nM for 2.5 h, and then treated with ethanol or CHX for an additional 1.5 h. qRT-PCR results showed that at this ASO concentration, 56 out of the 80 ASOs could reduce the *NCL* mRNA level by >40%, with ASO110080 and ASO110074 being the most active ASOs. Importantly, 36 active ASOs showed increased activity ($P < 0.05$) upon translation inhibition, although to different degrees. Interestingly, all the ASOs with enhanced activity target the coding region sequences. To confirm this observation, three ASOs were tested in a more detailed dose response study, including 110055 (Figure 6B), 110074 (Figure 6C, and 110080 as a positive control (Figure 6D). CHX treatment enhanced the activity of all the three ASOs. In addition to the tested 5–10–5 PS/MOE gapmer ASOs, CHX treatment also increased the activity of 5–10–5 PS/Me or PS/cEt gapmer ASOs targeting the ASO110074 site of *NCL* mRNA, but not the ASOs targeting the ASO116847 site of *PTEN* mRNA (Supplementary Figure S8), suggesting that translation can affect the behavior of ASOs with other chemical modifications, likely due to the high ability of ribosomes to resolve the RNA structures and even hybrid structures created by ASOs with very high affinity for nucleotides such as 2′-cEt modified ASOs. Together, these results indicate that the observed translation effect was not unique to ASO110080, and that the activity of many ASOs targeting the coding region of *NCL* mRNA can be enhanced by translation inhibition.

However, reduced ASO activity was observed upon translation inhibition for certain regions within the coding sequence, as shown for the underlined region (Figure 6A). Eight ASOs targeting this region showed reduced activity (from ASO110084 to ASO110091). This reduced activity was further confirmed in a dose response study for ASO110091 (Figure 6E), suggesting that this mRNA region may have reduced accessibility upon translation inhibition (see below).

After CHX treatment, the activity of the ASOs targeting the 5′ UTR appeared to be reduced (Figure 6A). However, the activities of these ASOs were generally poor, leading us to omit these ASOs in following studies. One the other hand, three of the four tested ASOs targeting the 3′ UTR exhibited decent activity (with >50% mRNA reduction). Interestingly, the activities of these 3′ UTR-targeting ASOs were reduced in CHX treated cells. This observation was further confirmed in dose–response studies for two ASOs, 110126 (Figure 6F) and 110128 (Figure 6G). Together, these results indicate that for the efficiently translated *NCL* mRNA, translation inhibition can enhance the activity of many, but not all, ASOs targeting the coding region, whereas the activity of ASOs targeting the 3′ UTR tends to be reduced (see below).

The *NCL* mRNA coding region showing reduced ASO activity has decreased accessibility upon translation inhibition

Although many ASOs targeting the coding region of *NCL* mRNA have enhanced activity upon translation inhibition, some ASOs targeting certain region of the coding sequence displayed reduced activity. It is possible that this particular region may have reduced accessibility upon translation inhibition, due to, for example, conformational change. To evaluate this possibility, an siRNA with the same sequence as ASO110086 was tested. As both siRNA and ASO trigger RNA degradation through base-pairing with target RNA but via different mechanisms, i.e. RISC and RNase H1 pathways, respectively, altered accessibility should affect the activities of both siRNA and ASO. Indeed, reduced activity was observed for both ASO110086 and siRNA-110086 upon CHX treatment (Figure 7A and B). As a control, the activity of a siRNA targeting the same site as ASO110074 was not altered by translation inhibition (Figure 7C), indicating that the RISC pathway was not affected by CHX treatment. These results together suggest an altered accessibility of the ASO110086 target region.

To further confirm a reduced accessibility, mRNA structure was analyzed by in vivo chemical modification using dimethyl sulfate (DMS), which methylates accessible A and C nucleotides and causes primer extension to stop one nucleotide before the modified nucleotides (66). Primer extension results showed that upon CHX treatment, many nucleotides in this region exhibited reduced accessibility to DMS (Figure 7D and E), as evidenced by the weaker signal intensities in CHX treated sample. The reduced accessibility seems not be due to stalled ribosomes in this region by CHX treatment, which causes translation arrest, since puromycin treatment also led to similar reduction in accessibility (Figure 7D). Puromycin inhibits translation by causing premature peptide release and dissociation of elongation ribosomes (56). Indeed, upon puromycin treatment, *NCL* mRNA was shifted toward 80S monosomes, and 18S and 28S rRNAs were substantially reduced from the polysome regions (Supplementary Figure S9A). In addition, modest reduction in activity was also observed for ASO110091 or an siRNA targeting the same site as ASO110091 upon puromycin treatment (Supplementary Figure S9B).

To determine if the mRNA region showing enhanced ASO activity upon translation inhibition has altered accessibility, we attempted but failed to test the CHX effect on an siRNA targeting the ASO110080 site, since this siRNA was inactive (Supplementary Figure S10A). This is not surprising, as the active sites do not always overlap between ASOs and siRNAs (67). However, as described above (Figure 7C), for the ASO110074 targeting site, the activity of the siRNA was not affected by CHX treatment, whereas the ASO activity was enhanced. This observation suggests that

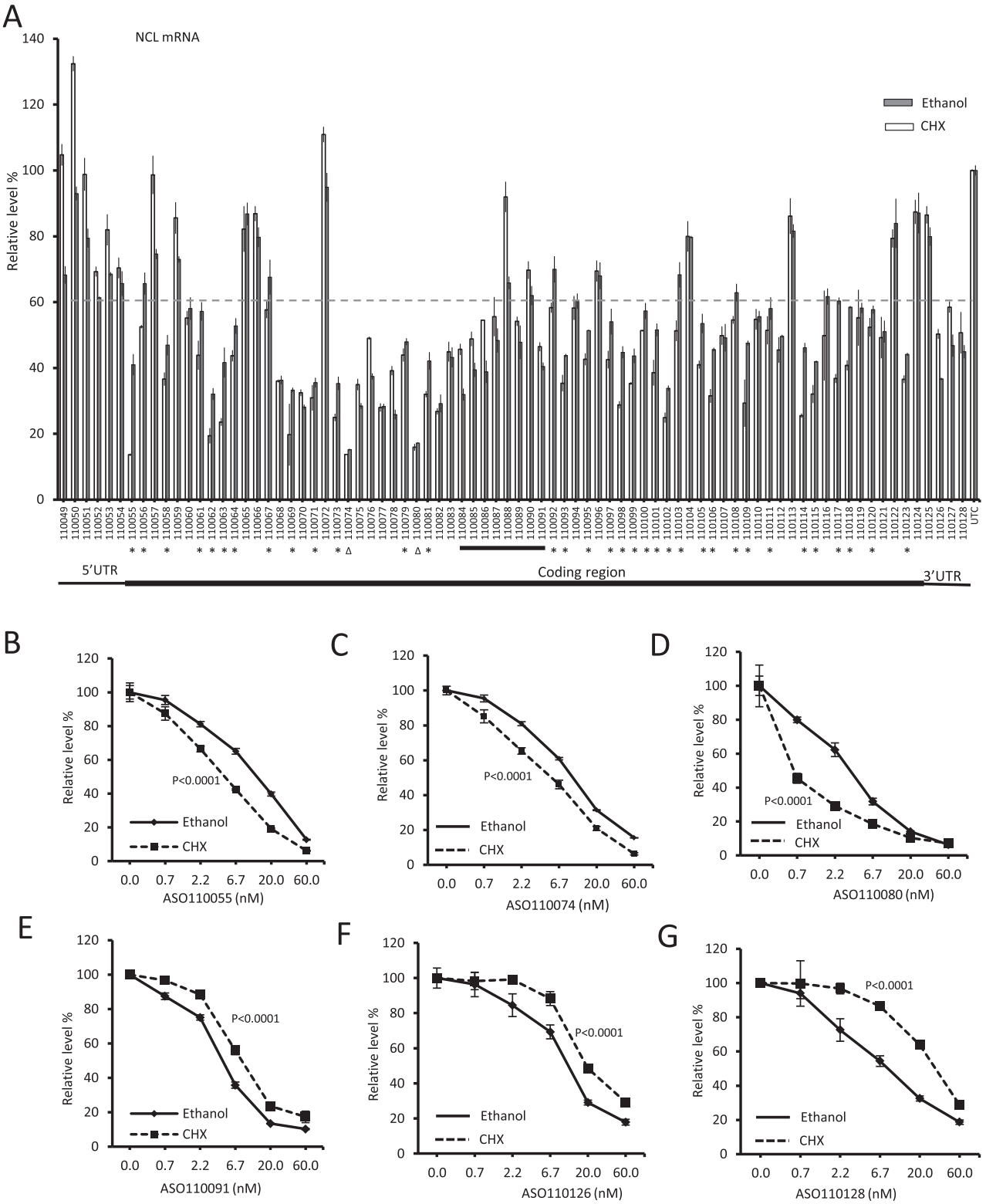

Figure 6. CHX treatment can enhance the activity of other ASOs targeting the coding region of *NCL* mRNA. (**A**) qRT-PCR quantification of *NCL* mRNA in HeLa cells transfected for 2.5 h with 15 nM ASOs, followed by treatment with ethanol or CHX for an additional 1.5 h. The ASO numbers are listed below X-axis. The UTRs and coding region of *NCL* mRNA are depicted. The underlined area exemplifies a region where reduced ASO activity was observed upon translation inhibition. The ASOs showing statistically significant increases in ASO activity upon CHX treatment are indicated by asterisks ($P < 0.05$). *P* values were calculated using *t*-test. The two ASOs showing significant increases in activity in other experiments are indicated by triangles. (**B–G**) qRT-PCR quantification of *NCL* mRNA in HeLa cells transfected with different ASOs for 2.5 h, followed by CHX treatment for 1.5 h. The error bars represent standard deviation of three experiments. *P*-values were calculated using *F*-test based on non-linear regression (curve fit) using Prism.

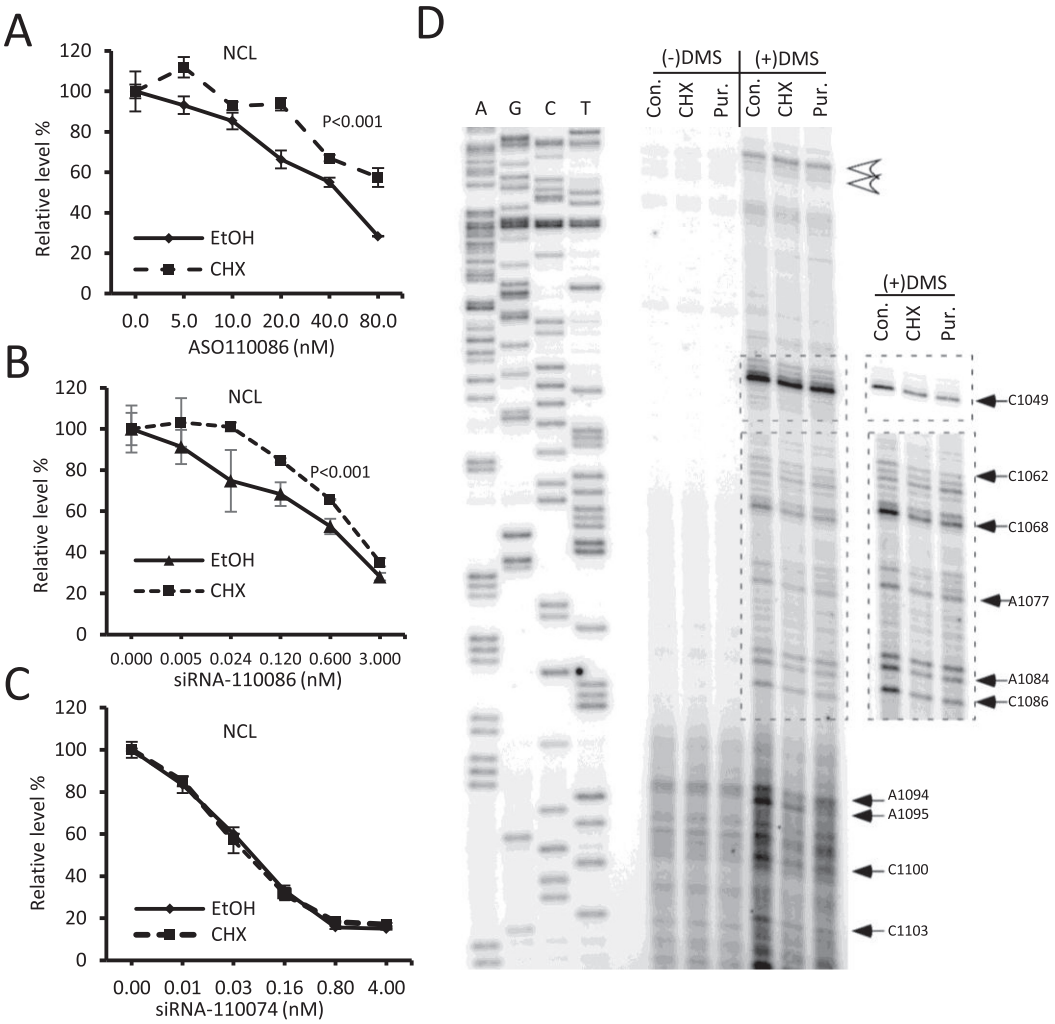

Figure 7. The coding region of *NCL* mRNA showing reduced ASO activity after translation inhibition has decreased accessibility. (**A**) qRT-PCR quantification of *NCL* mRNA in cells transfected with ASO110086, followed by CHX treatment. (**B**) qRT-PCR quantification of *NCL* mRNA in cells transfected with siRNA-110086 that target the same sequence as ASO110086, followed by CHX treatment. (**C**) qRT-PCR quantification of *NCL* mRNA in cells transfected with a siRNA targeting the same sequence as ASO110074, followed by CHX treatment. The error bars for these panels represent standard deviation of three experiments. *P*-values were calculated using *F*-test based on non-linear regression (curve fit) using Prism. (**D**) *In vivo* RNA structure probing using DMS modification and primer extension. Primer extension was performed using primer XL877 and extension products were separated on an 8% PAGE, next to DNA sequencing reactions performed with the same primer. The open arrows indicate extension products with similar signal intensity. The dash boxed regions were exemplified with different exposure times for better presentation. The nucleotides showing altered accessibility are indicated. Con., Control ethanol treated cells; CHX, CHX treated cells; Pur., Puromycin treated cells. (**E**) partial sequence of *NCL* mRNA region showing reduced ASO activity after translation inhibition. The asterisks indicate the nucleotides with reduced accessibility. The ASO target sequences and the primer region used for the extension reaction are underlined. The numbering system is based on the sequence of NM_005381.2.

for this mRNA region with enhanced ASO activity, the accessibility was not substantially altered. This is supported by the results from in vivo structural probing using DMS (Supplementary Figure S10B and C). No significant difference in accessibility was observed between control and CHX treated samples in the ASO110080 target region of *NCL* mRNA. Together, these results suggest that the reduced ASO activity by translation inhibition can be caused by decreased accessibility, whereas the accessibility of the mRNA region showing enhanced ASO activity was not significantly altered.

Translation inhibition can enhance the activities of ASOs targeting other efficiently translated mRNAs

As described above, since *NCL* mRNA is more efficiently translated compared with *PTEN* mRNA, it is possible that the translating ribosomes may affect RNase H1 recruitment due to the short intervals in between two adjacent ribosomes for the efficiently translated *NCL* mRNA. If that is the case, it may also apply to other efficiently translated mRNAs. As shown in Figure 5, *NPM1* mRNA appeared to be efficiently translated, as the mRNA migration pattern was similar to that of *NCL* mRNA. We thus performed polysome profile analysis for HeLa cells by sucrose gradient fractionation, and determined the migration patterns of several additional mRNAs, based on available information of screened active ASOs, and previous reports of their translation efficiency in mouse cells (68). *NPM1* mRNA was again enriched in heavy polysome fractions, as compared with the migration pattern of ribosomes indicated by the 28S rRNA (Figure 8A and B). Three additional mRNAs, *ANXA2*, *La* and *SOD1* mRNAs, were also found to be mainly enriched in heavy polysome fractions toward the bottom of the gradients (Figure 8C, D and E, respectively), indicating that these mRNAs are efficiently translated.

Next, HeLa cells were transfected with ASOs targeting the coding regions of these mRNAs, followed by CHX treatment. CHX treatment enhanced the activities of two tested *NPM1* ASOs, although the two ASOs had different potency (Figure 8F). Similarly, CHX treatment increased the activities of two tested ASOs targeting *ANXA2* mRNA (Figure 8G). Moreover, enhanced activities were also observed for the ASOs targeting *La* (Figure 8H) and *SOD1* mRNAs (Figure 8I), consistent with results observed when targeting *NCL* mRNA. The enhanced activity for the *La* ASOs is also consistent with the results observed above (Figure 4C). Together, these data indicate that translation inhibition can also enhance the activities of ASOs targeting the coding regions of other efficiently translated mRNAs.

Translation inhibition tends to not enhance the activity of ASOs targeting less efficiently translated mRNAs

Next, we evaluated if ASOs targeting other less-efficiently translated mRNAs behave similarly as the ASO targeting *PTEN* mRNA, which is less-efficiently translated. Polysome profiles of seven additional mRNAs were analyzed using the same samples as in Figure 8. These mRNAs were chosen based on the available information of screened active ASOs, and translation efficiency as demonstrated previously in mouse cells (68). These include *AGO2*, *Drosha*, *ACP1*, *CDK7*, *CDC2*, *eIF4E* and *DPYSL2* mRNAs, which tend to be enriched in the 80S mono-ribosome and light polysome regions (Supplementary Figure S11). This is especially the case for *ACP1, CDK7, CDC2, eIF4E* and *DPYSL2* mRNAs. Although *AGO2* and *Drosha* mRNAs were enrichment in the polysome fractions as compared with *ACP1* mRNA, such enrichment was much weaker as compared with *NPM1* mRNA (Figure 8B). These results suggest that these mRNAs are less efficiently translated and are associated with one or fewer ribosomes per mRNA at a given time, as compared with that of *NCL* or *NPM1* mRNAs.

ASOs targeting the coding regions of these mRNAs were then tested into HeLa cells. Upon CHX treatment, the ASO activity was not enhanced for all the seven tested ASOs targeting these less-efficiently translated mRNAs (Figure 9A–G), similar to the *PTEN* ASO. As a control, the activity of the *NCL* ASO110080 was again increased in CHX treated cells (Figure 9H). Interestingly, the activities of the ASOs targeting *CDK7* (Figure 9E), *eIF4E* (Figure 9F) or *DPYSL2* (Figure 9G) were even decreased by inhibition of translation. To determine if the ASO target sites within these mRNAs had reduced accessibility upon CHX treatment, a siRNA with the same sequence as ASO183750 was designed to target *eIF4E* mRNA. Indeed, the activity of the *eIF4E* siRNA was also slightly reduced upon translation inhibition (Figure 9I), whereas another siRNA targeting *Drosha* mRNA did not (Figure 9J), once again suggesting that the RISC pathway was not impaired under these experimental conditions, and that the *eIF4E* ASO target site is likely less accessible. Together, these results from seven different mRNAs suggest that translation inhibition tends to not enhance the activity of ASOs targeting the less efficiently translated mRNAs. This is further supported by the observation that translation inhibition did not enhance the activity of six additional ASOs targeting different sequences within the coding region of *AGO2* mRNA (Supplementary Figure S12).

Translation inhibition tends to reduce the activity of ASOs targeting 3′ UTRs regardless of translation efficiency

As observed above, the activities of the three active *NCL* 3′ UTR ASOs were all reduced upon CHX treatment (Figure 6). To determine if this observation also applies to other 3′ UTR targeting ASOs, HeLa cells were transfected with ASOs targeting the 3′ UTRs of the efficiently translated *ANXA2, La,* and *SOD1* mRNAs, and the less-efficiently translated *AGO2, ACP1* and *DPYSL2* mRNAs. qRT-PCR results showed that upon CHX treatment, the activities of the two ASOs targeting the 3′ UTR of *ANXA2* mRNA were modestly reduced (Figure 10A and B). Similarly, reduced activities of ASOs targeting the 3′ UTRs of *La* (Figure 10C) and *SOD1* (Figure 10D) mRNAs were also observed upon translation inhibition. Further, the activities of ASOs targeting the 3′ UTRs of the less-efficiently translated *AGO2* (Figure 10E), *ACP1* (Figure 10F) and *DPYSL2* (Figure 10G) mRNAs were decreased after CHX treatment. In addition, the decreased activity of 3′ UTR ASOs was not specific to CHX, since 4E1Rcat, LTM, or Puromycin treatment also reduced the activities of 3′ UTR ASOs tar-

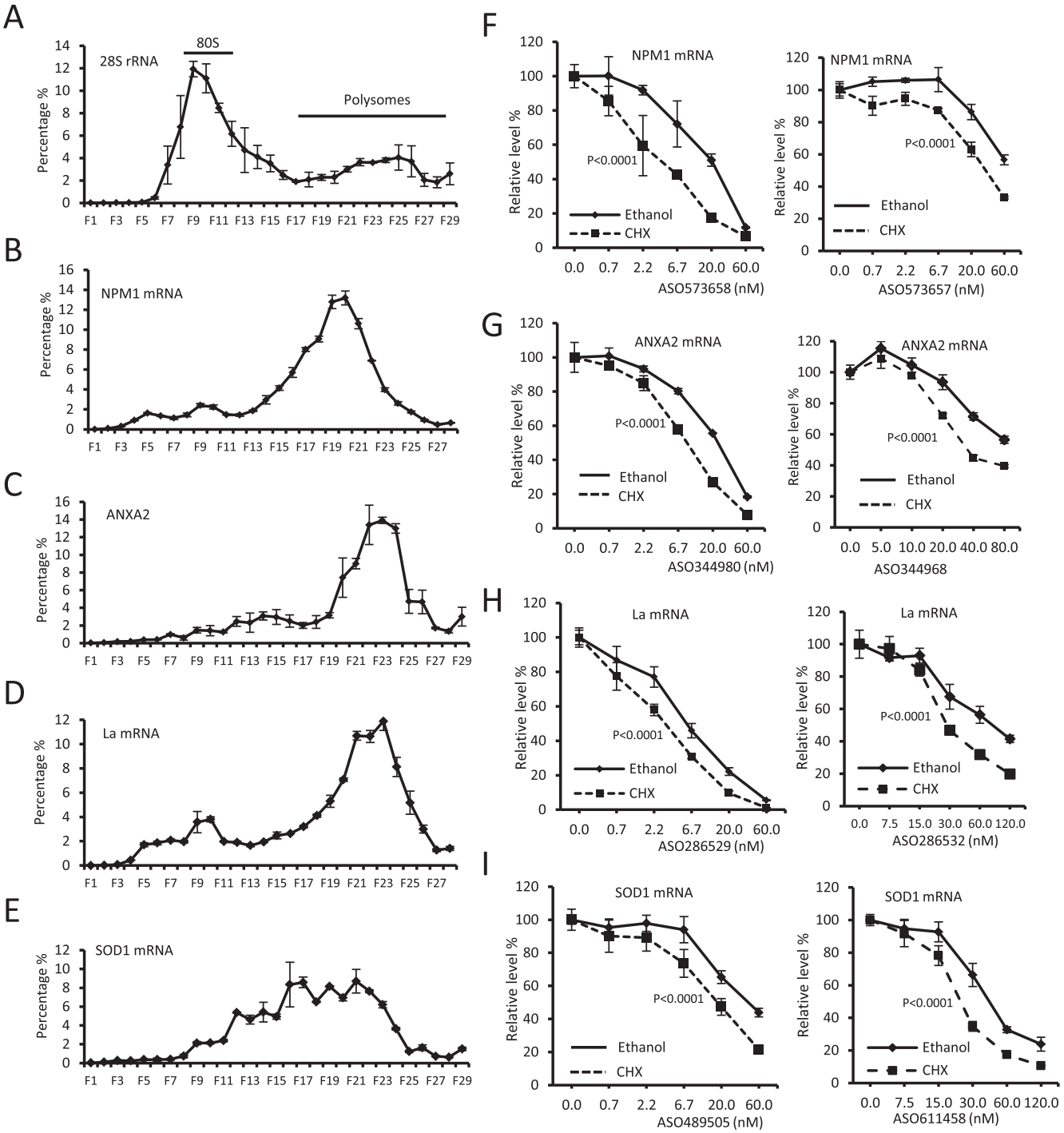

Figure 8. CHX treatment can increase the activities of ASOs targeting other efficiently translated mRNAs. qRT-PCR quantification of 28S rRNA **(A)**, *NPM1* (**B**), *ANXA2* (**C**), *La* (**D**) and *SOD1* (**E**) mRNAs in different sucrose gradient fractions. The percentages of the RNAs in each fraction were calculated and plotted. (F–I) HeLa cells were transfected for 2.5h with ASOs targeting *NPM1* (**F**), *ANXA2* (**G**), *La* (**H**) and *SOD1* (**I**) mRNAs, with two different ASOs for each mRNA, followed by CHX treatment for an additional 1.5 h. The corresponding mRNA levels were determined by qRT-PCR. The error bars represent standard deviation of three experiments. *P*-values were calculated using *F*-test based on non-linear regression (curve fit) using Prism.

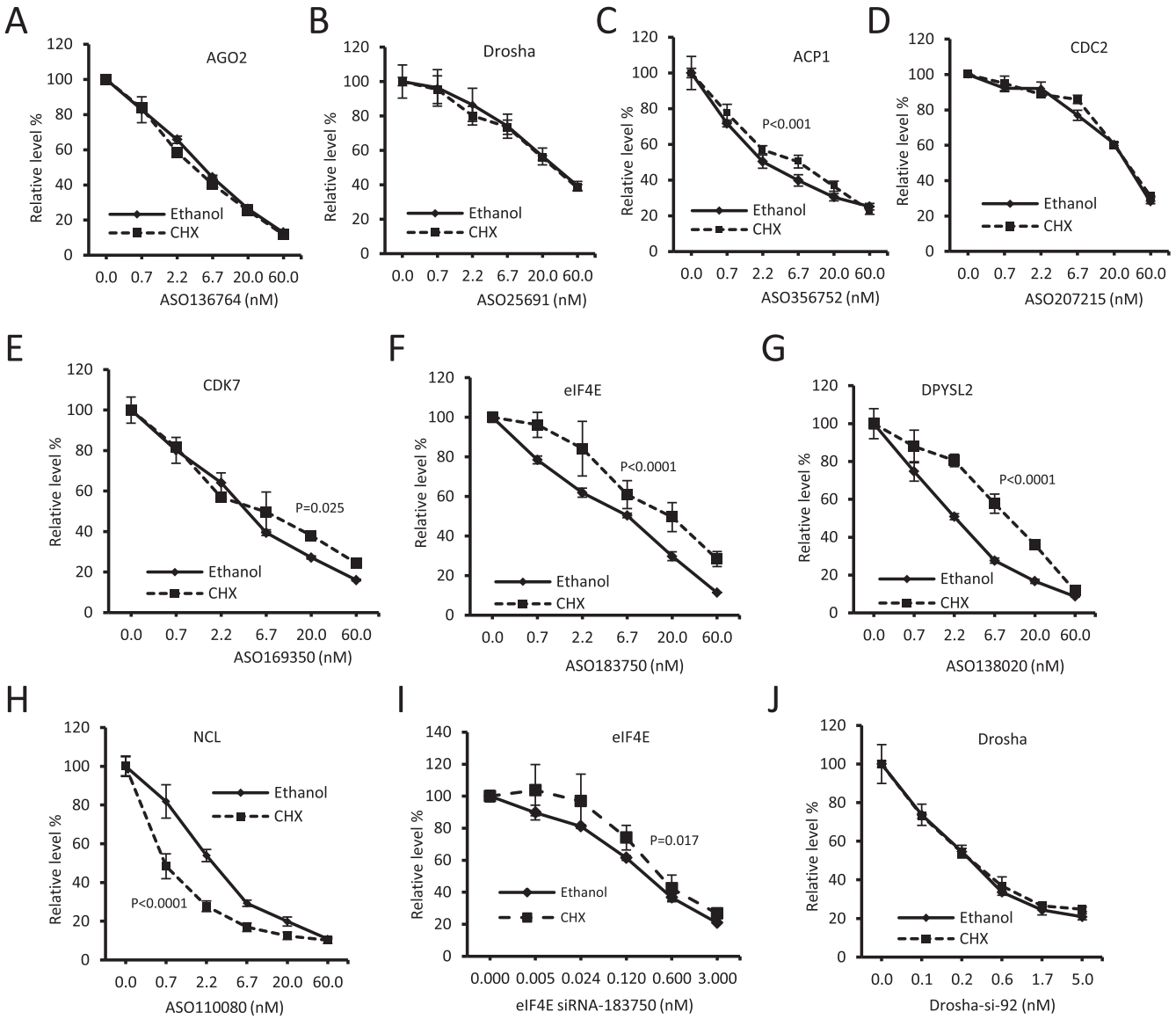

Figure 9. Translation inhibition tends to not enhance the activity of ASOs targeting less-efficiently translated mRNAs. HeLa cells were transfected with different ASOs for 2.5 h, followed by CHX treatment for an additional 1.5h. qRT-PCR was performed to determine the levels of targeted mRNAs, including *AGO2* (**A**), *Drosha* (**B**), *ACP1* (**C**), *CDC2* (**D**), *CDK7* (**E**), *EIF4E* (**F**) and *DPYSL2* (**G**) mRNAs. (**H**) qRT-PCR quantification of *NCL* mRNA in cells treated with ASO110080 that served as a positive control for CHX treatment. (**I**) qRT-PCR quantification of *eIF4E* mRNA in HeLa cells transfected for 2.5 h with an siRNA targeting the same site as ASO183570, followed by CHX treatment. (**J**) qRT-PCR quantification of *Drosha* mRNA in HeLa cells treated with a *Drosha*-specific siRNA, followed by CHX treatment, as in panel I. The error bars represent standard deviation of three experiments. *P*-values were calculated using *F*-test based on non-linear regression (curve fit) using Prism.

geting *NCL* (Supplementary Figure S13A) or *La* (Supplementary Figure S13B). The accessibility of the 3′ UTRs appeared to be reduced upon translation inhibition, as siRNAs targeting the 3′ UTR of *NCL* mRNA at same sites targeted by ASO110126 or ASO110128 also showed reduced activity (Figure 10H and I). Together, these results indicate that translation inhibition tends to reduce the ASO activity when targeting the 3′ UTRs, in a manner independent of the mRNA translation efficiency.

DISCUSSION

Understanding the cellular mechanisms that affect ASO activity is important for the design of better antisense drugs, and for interpretation of results obtained using ASO-mediated modulation of gene expression. Previous studies have shown that many factors can affect ASO activity, such as cellular ASO uptake, intracellular distribution, protein binding, target RNA localization and local structure, as well as RNA stability (2,10,12,16–21). Here, we show that the translation process can also affect the activity of ASOs in triggering target mRNA reduction. Translation inhibition using different approaches tends to increase the activ-

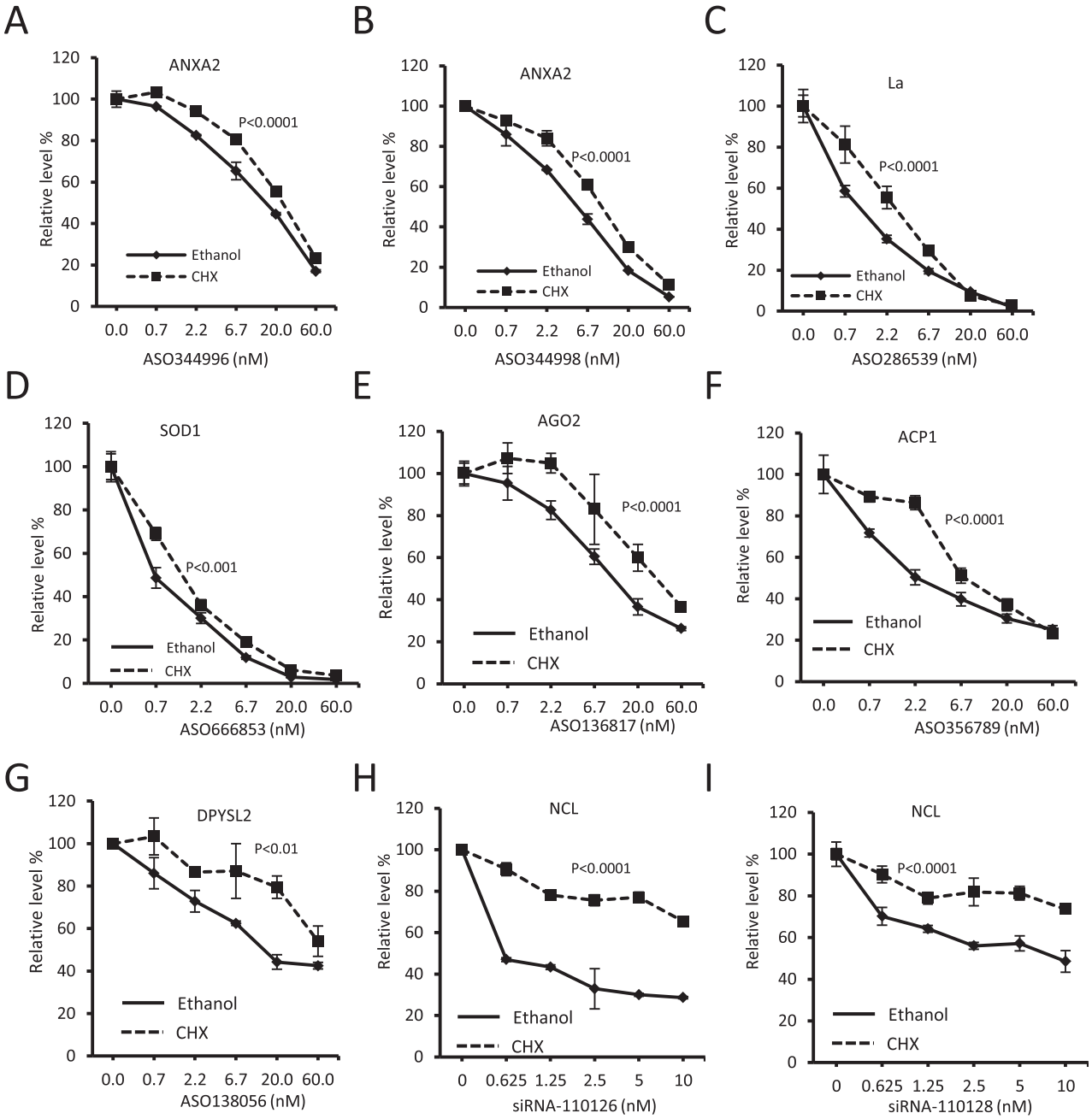

Figure 10. ASOs targeting 3′ UTRs tend to have reduced activity upon translation inhibition. HeLa cells were transfected with different ASOs for 2.5h, followed by CHX treatment for an additional 1.5h. qRT-PCR was performed to determine the levels of the targeted mRNAs, including the efficiently translated *ANXA2* (**A** and **B**), *La* (**C**), *SOD1* (**D**) mRNAs, and less-efficiently translated *AGO2* (**E**), *ACP1* (**F**), and *DPYSL2* (**G**) mRNAs. (**H**) qRT-PCR quantification of *NCL* mRNA in HeLa cells transfected for 2.5 h with an siRNA targeting the same sequence as ASO110126, followed by CHX treatment for an additional 1.5 h. (**I**) qRT-PCR quantification of *NCL* mRNA in HeLa cells treated as in panel H, but with an siRNA targeting the same sequence as ASO110128. The error bars represent standard deviation of three experiments. *P*-values were calculated using F-test based on non-linear regression (curve fit) using Prism.

ity of ASOs targeting the coding regions of efficiently translated mRNAs, but not the less-efficiently translated mRNAs or nuclear non-coding RNA and pre-mRNA. To our knowledge, this is the first time that a relatively precise site (polysomes) of intracellular ASO activity has been demonstrated. These observations further demonstrate robust cytoplasmic activity of RNase H1-dependent ASOs, as recently reported using kinetics and fractionation studies (9). Indeed, ASO-mediated mRNA cleavage products were co-isolated with ribosomes, which are normally enriched in the cytoplasm, further indicating that ASOs can trigger RNase H1 cleavage in the cytoplasm, in addition to the nucleus.

The effects of translation inhibitors on ASO activity appear to result from stalled or slowed translation, and not from non-specific effects related to the drugs. Treatment for 1.5 h with CHX that inhibits translation elongation signif-

icantly enhanced the *NCL* ASO110080 activity. Under this experimental condition, the levels of tested proteins known to be important for ASO activity were not altered, and ASO transfection and subcellular distribution were also unaffected, suggesting that changes in ASO activity was not due to unexpected global effects related to the CHX treatment. This is further supported by the observations that the activities of other ASOs targeting Malat1 or some less efficiently translated mRNAs (e.g. *AGO2* and *Drosha*) were not affected under the same conditions. In addition, similar effects on ASO activities were observed using different translation inhibitors, including 4E1Rcat, puromycin, and LTM, which inhibit translation via different mechanisms. More importantly, specific inhibition of *NCL* mRNA translation using an oligonucleotide also specifically enhanced the activity of the *NCL* ASO. Together, these results indicate that the stalled or slowed translation led to the enhanced activity of the ASO targeting the efficiently translated *NCL* mRNA.

Enhanced activity by translation inhibition was also observed for different ASOs targeting the coding regions of four additional efficiently translated mRNAs, including *La, NPM1, SOD1*, and *ANXA2*, indicating that the observed effect was not unique to *NCL* mRNA. In addition to 5–10–5 PS/MOE ASO, CHX treatment also enhanced the activity of *NCL* ASOs, and not PTEN or Malat1 ASOs, with 5–10–5 PS/Me or PS/cEt ASO design, suggesting that the effect of translation on ASO activity is not unique to a single chemical modification. However, we cannot exclude the possibility that some ASOs with different chemical modifications may have different responses to translation inhibition, due to altered affinity for mRNA target or altered protein binding profiles. The ASO activity was increased to different degrees for different ASOs targeting these mRNAs, suggesting that many factors, such as differences in translate rates or local mRNA structures, can act in concert to affect final ASO activity. This complexity was more evident when multiple ASOs were tested to target different regions of *NCL* mRNA. Although a majority of the active ASOs targeting the coding region showed enhanced activity after translation inhibition, reduced activity was observed for several ASOs targeting certain positions of the coding region of *NCL* mRNA, due to decreased accessibility.

When targeting less efficiently translated mRNAs, no enhancement in ASO activity was observed upon translation inhibition for seven tested mRNAs, including *PTEN, AGO2, Drosha, CDK7, eIF4E, ACP1* and *DPYSL2*, and for all the seven tested ASOs targeting different sequences within the coding region of *AGO2* mRNA. Contrarily, reduced activity was observed for the tested ASOs targeting *ACP1, CDK7*, *eIF4E* and *DPYSL2* mRNAs, likely due to reduced accessibility. Although we cannot exclude the possibility that enhanced activities might be observed upon translation inhibition for certain ASO(s) targeting these less-efficiently translated mRNAs when more ASOs are tested, our current results suggest that the activity of ASOs targeting less-efficiently translated mRNAs tends to remain unchanged or decline.

These observations together suggest a possibility that for the less-efficiently translated mRNAs, the interval between two adjacent translating ribosomes might be long enough to avoid being a limiting factor for ASO binding and RNase H1 recruitment (Figure 11A). However, for the efficiently translated mRNAs loaded with more ribosomes per mRNA, the interval between two adjacent ribosomes is relatively short, which may allow the translating ribosome to interfere with ASO binding and/or RNase H1 recruitment (Figure 11B). This model is supported by the observation that upon RNase H1 over-expression, CHX treatment could not further enhance ASO activity, suggesting that RNase H1 recruitment might be a limiting factor when targeting certain mRNAs or positions. In addition, it is also supported by the observation that the enhanced activity of ASO110080 was not due to increased mRNA accessibility upon translation inhibition.

The observations for 3′ UTR ASOs also support the potential influence of translating ribosome on ASO activity. Although ASOs targeting the coding regions of efficiently translated mRNAs (e.g. *NCL*) tend to increase activity upon translation inhibition, this was not observed for the 3′ UTR ASOs. Since 3′ UTR is usually not scanned by the ribosomes, translation efficiency in theory should not affect ASOs targeting this region. Indeed, no enhanced activity was observed for 11 tested ASOs targeting the 3′ UTRs of seven different mRNAs, regardless of the transla-

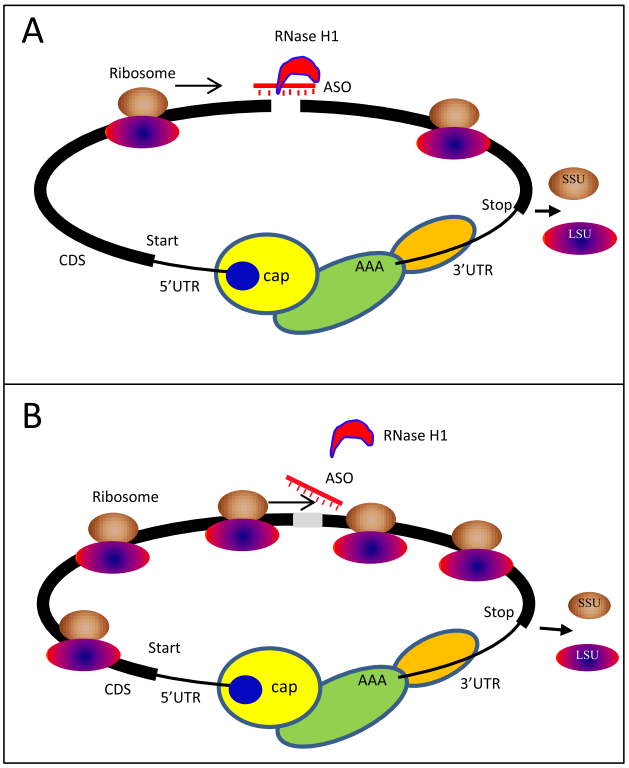

Figure 11. Proposed model of translation effects on ASO action. (**A**) Less-efficiently translated mRNAs. The coding region sequence (CDS) is shown in thick lines, and UTRs are in thin lines and indicated. The ribosome subunits are shown. Proteins that bind 5′cap, poly(A), and 3′ UTR are depicted. An ASO base-pairing with the mRNA target can recruit RNase H1 to cleave the target mRNA. SSU, small subunit; LSU, large subunit. (**B**) Efficiently translated mRNAs. The heavily loaded ribosomes are indicated. The limited interval between two adjacent ribosomes may not be sufficient for RNase H1 recruitment if the recruitment rate is limited, thus may cause some ASOs being removed from mRNA by the ribosome.

tion efficiency. Interestingly, the activities of 3′ UTR ASOs tend to be reduced upon translation inhibition, most likely due to decreased accessibility, as supported by the observations that siRNAs targeting the same sites in *NCL* 3′ UTR also showed reduced activity. Currently it is not clear how 3′ UTR structure or composition of the mRNP changes upon translation inhibition that tends to reduce ASO activity. 3′ UTR can associate with many regulatory factors, such as proteins and miRNPs and can be looped with 5′ UTR (27,37). It is therefore possible that translation inhibition may somehow enhance or stabilize such interactions, leading to reduced accessibility to ASOs and siRNAs. Detailed understanding of the changes of 3′ UTR features upon translation modulation requires further investigation.

Although translation inhibition can enhance the activity of RNase H1-dependent ASOs targeting the coding region of *NCL* mRNA, under the same condition, the effect of translation inhibition on the activity of siRNA targeting the same site might be different. For example, increased activity was observed for ASO110074 upon CHX treatment, but not for the siRNA targeting the same site (Figure 9J). It is possible that siRNA base-pairs with target RNA in a preloaded form, i.e., already associated with the endonuclease AGO2 before binding to target RNA (69). Once bound, siRNA can immediately trigger cleavage of the mRNA. For ASOs, RNase H1 needs to be recruited after ASO binding to the target RNA (1), therefore it may require longer time than siRNA to trigger target cleavage. This longer time requirement for ASO action may thus increase the chance to be affected by the translating ribosomes. Understanding the exact mechanisms causing the different response to translation inhibition between siRNAs and ASOs may help to explain why in some cases the active target sites within mRNAs do not always overlap between ASOs and siRNAs (67,70).

The different activity changes of ASOs targeting different mRNAs or different positions of the same mRNA upon translation inhibition are interesting. This further highlights the complexity of mRNA structures in combination with translation events. Similarly, this complex effect was also observed for siRNAs. For example, no activity change was observed for siRNAs targeting certain coding regions of *NCL* or *Drosha* mRNAs, whereas reduced activity was observed for siRNAs targeting the ASO110086-binding region and the 3′ UTR of *NCL* mRNA or the coding region of *eIF4E* mRNA. In the latter cases, reduced activities were also observed for ASOs targeting the same sites, suggesting that the reduced activity was not specific to a particular mechanism, rather, it was more likely resulted from altered accessibility of the local RNA sites. These observations may partially explain previous controversial results regarding siRNA activity upon translation inhibition. For instance, enhanced siRNA activity was detected upon translation inhibition when targeting a *EGFP* reporter mRNA (71), yet reduced activity was found in other studies for other RNAs (72). These different observations might stem from different RNA conformational changes upon translation inhibition for different target sites or different mRNAs. However, other factors may also contribute to these different behaviors of different siRNAs, such as experimental conditions.

Together, our results suggest that translation efficiency can affect ASO activity when targeting coding regions, likely due to the short intervals between translating ribosomes. This effect may contribute to the variations in ASO activity in different cell types or in different tissues, as mRNA translation efficiency may be different. However, even for efficiently translated mRNAs, active ASOs can still be identified when targeting the coding regions, as exemplified for the *NCL* mRNA (Figure 6), suggesting that translation efficiency may not be a major factor to limit ASO activity, at least for the ASOs tested in this study. This is not surprising, since many factors can affect ASO activity at different steps during ASO action, and different ASOs may be affected differently by each factor. On the other hand, active ASOs may also be identified in the 3′ UTR region, where translating ribosome may not affect ASO activity. Thus, experimental screening of ASOs is needed for identification of the most potent ASOs. Nonetheless, our results suggest that biological processes like translation can affect ASO activity, and further understanding the effects of biological events on ASO performance will be valuable to guide better drug design as well as to provide insights that may explain inactive or less active ASOs. Moreover, this and other studies (9,10,19,21) provide additional knowledge that should assist better controlled experiments and more sophisticated interpretations of experimental results. Finally, these results further support previous studies that showed that RNase H1 recruitment is frequently the rate limiting step in the activity of RNase H1-activating ASOs (10,20,21).

SUPPLEMENTARY DATA

Supplementary Data are available at NAR Online.

ACKNOWLEDGEMENTS

The authors wish to thank Wen Shen, Shiyu Wang and Tim Vickers for discussions.

FUNDING

Ionis Pharmaceuticals. Funding for open access charge: Ionis Pharmaceuticals.
Conflict of interest statement. All authors are employees of Ionis Pharmaceuticals.

REFERENCES

1. Crooke,S.T., Vickers,T.A., Lima,W.F. and Wu,H.-J. (2008) In: Crooke,ST (ed). *Antisense Drug Technology - Principles, Strategies, and Applications*. 2nd edn. CRC Press, Boca Raton, pp. 3–46.
2. Dias,N. and Stein,C.A. (2002) Antisense oligonucleotides: basic concepts and mechanisms. *Mol Cancer Ther*, **1**, 347–355.
3. Swayze,E.E. and Bhat,B. (2008) In: Crooke,ST (ed). *Antisense Drug Technology—Principles, Strategies, and Applications*. 2nd edn. CRC Press, Boca Raton, pp. 143–182.
4. Geary,R.S., Norris,D., Yu,R. and Bennett,C.F. (2015) Pharmacokinetics, biodistribution and cell uptake of antisense oligonucleotides. *Adv. Drug Deliv. Rev.*, **87**, 46–51.
5. Lima,W., Wu,H. and Crooke,S.T. (2008) In: Crooke,ST (ed). *Antisense Drug Technology—Principles, Strategies, and Applications*. 2nd edn. CRC Press, Boca Raton, pp. 47–74.

6. Wu,H., Sun,H., Liang,X.H., Lima,W.F. and Crooke,S.T. (2013) Human RNase H1 is associated with protein P32 and is involved in mitochondrial pre-rRNA processing. *PLoS One*, **8**, e71006.
7. Wu,H., Lima,W.F., Zhang,H., Fan,A., Sun,H. and Crooke,S.T. (2004) Determination of the role of the human RNase H1 in the pharmacology of DNA-like antisense drugs. *J. Biol. Chem.*, **279**, 17181–17189.
8. Lima,W.F., Murray,H.M., Damle,S.S., Hart,C.E., Hung,G., De Hoyos,C.L., Liang,X.H. and Crooke,S.T. (2016) Viable RNaseH1 knockout mice show RNaseH1 is essential for R loop processing, mitochondrial and liver function. *Nucleic Acids Res.*, **44**, 5299–5312.
9. Liang,X.H., Sun,H., Nichols,J.G. and Crooke,S.T. (2017) RNase H1-dependent antisense oligonucleotides are robustly active in directing RNA cleavage in both the cytoplasm and the nucleus. *Mol. Ther.*, **25**, 2075–2092.
10. Vickers,T.A. and Crooke,S.T. (2015) The rates of the major steps in the molecular mechanism of RNase H1-dependent antisense oligonucleotide induced degradation of RNA. *Nucleic Acids Res.*, **43**, 8955–8963.
11. Bennett,C.F. and Swayze,E.E. (2010) RNA targeting therapeutics: molecular mechanisms of antisense oligonucleotides as a therapeutic platform. *Annu. Rev. Pharmacol. Toxicol.*, **50**, 259–293.
12. Crooke,S.T., Wang,S., Vickers,T.A., Shen,W. and Liang,X.H. (2017) Cellular uptake and trafficking of antisense oligonucleotides. *Nat. Biotech.*, **35**, 230–237.
13. Wang,S., Sun,H., Tanowitz,M., Liang,X.H. and Crooke,S.T. (2016) Annexin A2 facilitates endocytic trafficking of antisense oligonucleotides. *Nucleic Acids Res.*, **44**, 7314–7330.
14. Wang,S., Sun,H., Tanowitz,M., Liang,X.H. and Crooke,S.T. (2017) Intra-endosomal trafficking mediated by lysobisphosphatidic acid contributes to intracellular release of phosphorothioate-modified antisense oligonucleotides. *Nucleic Acids Res.*, **45**, 5309–5322.
15. Juliano,R.L. and Carver,K. (2015) Cellular uptake and intracellular trafficking of oligonucleotides. *Adv. Drug Deliv. Rev.*, **87**, 35–45.
16. Bennett,C.F., Baker,B.F., Pham,N., Swayze,E. and Geary,R.S. (2016) Pharmacology of antisense drugs. *Annu. Rev. Pharmacol. Toxicol.*, **57**, 81–105.
17. Castanotto,D., Lin,M., Kowolik,C., Wang,L., Ren,X.Q., Soifer,H.S., Koch,T., Hansen,B.R., Oerum,H., Armstrong,B. *et al.* (2015) A cytoplasmic pathway for gapmer antisense oligonucleotide-mediated gene silencing in mammalian cells. *Nucleic Acids Res.*, **43**, 9350–9361.
18. Liang,X.H., Shen,W., Sun,H., Prakash,T.P. and Crooke,S.T. (2014) TCP1 complex proteins interact with phosphorothioate oligonucleotides and can co-localize in oligonucleotide-induced nuclear bodies in mammalian cells. *Nucleic Acids Res.*, **42**, 7819–7832.
19. Liang,X.H., Sun,H., Shen,W. and Crooke,S.T. (2015) Identification and characterization of intracellular proteins that bind oligonucleotides with phosphorothioate linkages. *Nucleic Acids Res.*, **43**, 2927–2945.
20. Vickers,T.A. and Crooke,S.T. (2014) Antisense oligonucleotides capable of promoting specific target mRNA reduction via competing RNase H1-dependent and independent mechanisms. *PLoS One*, **9**, e108625.
21. Lima,W.F., Vickers,T.A., Nichols,J., Li,C. and Crooke,S.T. (2014) Defining the factors that contribute to on-target specificity of antisense oligonucleotides. *PLoS One*, **9**, e101752.
22. Bennett,C.F., Chiang,M.Y., Chan,H., Shoemaker,J.E. and Mirabelli,C.K. (1992) Cationic lipids enhance cellular uptake and activity of phosphorothioate antisense oligonucleotides. *Mol. Pharmacol.*, **41**, 1023–1033.
23. Liang,X.H., Vickers,T.A., Guo,S. and Crooke,S.T. (2011) Efficient and specific knockdown of small non-coding RNAs in mammalian cells and in mice. *Nucleic Acids Res.*, **39**, e13.
24. Zong,X., Huang,L., Tripathi,V., Peralta,R., Freier,S.M., Guo,S. and Prasanth,K.V. (2015) Knockdown of nuclear-retained long noncoding RNAs using modified DNA antisense oligonucleotides. *Methods Mol. Biol.*, **1262**, 321–331.
25. Sharp,P.A. (2005) The discovery of split genes and RNA splicing. *Trends Biochem. Sci.*, **30**, 279–281.
26. Oeffinger,M. and Zenklusen,D. (2012) To the pore and through the pore: a story of mRNA export kinetics. *Biochim. Biophys. Acta*, **1819**, 494–506.
27. Jackson,R.J., Hellen,C.U. and Pestova,T.V. (2010) The mechanism of eukaryotic translation initiation and principles of its regulation. *Nat. Rev. Mol. Cell Biol.*, **11**, 113–127.
28. Hinnebusch,A.G. (2014) The scanning mechanism of eukaryotic translation initiation. *Annu. Rev. Biochem.*, **83**, 779–812.
29. Alekhina,O.M. and Vassilenko,K.S. (2012) Translation initiation in eukaryotes: versatility of the scanning model. *Biochemistry (Mosc.)*, **77**, 1465–1477.
30. Poole,E. and Tate,W. (2000) Release factors and their role as decoding proteins: specificity and fidelity for termination of protein synthesis. *Biochim. Biophys. Acta*, **1493**, 1–11.
31. Pisareva,V.P., Pisarev,A.V., Komar,A.A., Hellen,C.U. and Pestova,T.V. (2008) Translation initiation on mammalian mRNAs with structured 5′UTRs requires DExH-box protein DHX29. *Cell*, **135**, 1237–1250.
32. Qu,X., Wen,J.D., Lancaster,L., Noller,H.F., Bustamante,C. and Tinoco,I. Jr (2011) The ribosome uses two active mechanisms to unwind messenger RNA during translation. *Nature*, **475**, 118–121.
33. Noll,H. (2008) The discovery of polyribosomes. *BioEssays*, **30**, 1220–1234.
34. Warner,J.R. and Knopf,P.M. (2002) The discovery of polyribosomes. *Trends Biochem. Sci.*, **27**, 376–380.
35. Hinnebusch,A.G., Ivanov,I.P. and Sonenberg,N. (2016) Translational control by 5′-untranslated regions of eukaryotic mRNAs. *Science*, **352**, 1413–1416.
36. Wethmar,K. (2014) The regulatory potential of upstream open reading frames in eukaryotic gene expression. *Wiley Interdiscip. Rev. RNA*, **5**, 765–778.
37. Sonenberg,N. and Hinnebusch,A.G. (2009) Regulation of translation initiation in eukaryotes: mechanisms and biological targets. *Cell*, **136**, 731–745.
38. Yamashita,A. and Takeuchi,O. (2017) Translational control of mRNAs by 3′-Untranslated region binding proteins. *BMB Rep.*, **50**, 194–200.
39. Fabian,M.R., Sonenberg,N. and Filipowicz,W. (2010) Regulation of mRNA translation and stability by microRNAs. *Annu. Rev. Biochem.*, **79**, 351–379.
40. Imataka,H., Gradi,A. and Sonenberg,N. (1998) A newly identified N-terminal amino acid sequence of human eIF4G binds poly(A)-binding protein and functions in poly(A)-dependent translation. *EMBO J.*, **17**, 7480–7489.
41. Yu,C.H., Dang,Y., Zhou,Z., Wu,C., Zhao,F., Sachs,M.S. and Liu,Y. (2015) Codon usage influences the local rate of translation elongation to regulate co-translational protein folding. *Mol. Cell*, **59**, 744–754.
42. MacKay,V.L., Li,X., Flory,M.R., Turcott,E., Law,G.L., Serikawa,K.A., Xu,X.L., Lee,H., Goodlett,D.R., Aebersold,R. *et al.* (2004) Gene expression analyzed by high-resolution state array analysis and quantitative proteomics: response of yeast to mating pheromone. *Mol. Cell. Proteomics: MCP*, **3**, 478–489.
43. Qin,X., Ahn,S., Speed,T.P. and Rubin,G.M. (2007) Global analyses of mRNA translational control during early Drosophila embryogenesis. *Genome Biol.*, **8**, R63.
44. Zenklusen,D., Larson,D.R. and Singer,R.H. (2008) Single-RNA counting reveals alternative modes of gene expression in yeast. *Nat. Struct. Mol. Biol.*, **15**, 1263–1271.
45. Dana,A. and Tuller,T. (2012) Determinants of translation elongation speed and ribosomal profiling biases in mouse embryonic stem cells. *PLoS Comput. Biol.*, **8**, e1002755.
46. Ingolia,N.T., Lareau,L.F. and Weissman,J.S. (2011) Ribosome profiling of mouse embryonic stem cells reveals the complexity and dynamics of mammalian proteomes. *Cell*, **147**, 789–802.
47. Brocchieri,L. and Karlin,S. (2005) Protein length in eukaryotic and prokaryotic proteomes. *Nucleic Acids Res.*, **33**, 3390–3400.
48. Wu,B., Eliscovich,C., Yoon,Y.J. and Singer,R.H. (2016) Translation dynamics of single mRNAs in live cells and neurons. *Science*, **352**, 1430–1435.
49. Liang,X.H., Shen,W., Sun,H., Migawa,M.T., Vickers,T.A. and Crooke,S.T. (2016) Translation efficiency of mRNAs is increased by antisense oligonucleotides targeting upstream open reading frames. *Nat. Biotech.*, **34**, 875–880.
50. Schneider-Poetsch,T., Ju,J., Eyler,D.E., Dang,Y., Bhat,S., Merrick,W.C., Green,R., Shen,B. and Liu,J.O. (2010) Inhibition of eukaryotic translation elongation by cycloheximide and lactimidomycin. *Nat. Chem. Biol.*, **6**, 209–217.

51. Boisvert,F.M., Ahmad,Y., Gierlinski,M., Charriere,F., Lamont,D., Scott,M., Barton,G. and Lamond,A.I. (2012) A quantitative spatial proteomics analysis of proteome turnover in human cells. *Mol. Cell. Proteomics: MCP*, **11**, doi:10.1074/mcp.M111.011429.
52. Ignowski,J.M. and Schaffer,D.V. (2004) Kinetic analysis and modeling of firefly luciferase as a quantitative reporter gene in live mammalian cells. *Biotechnol. Bioeng.*, **86**, 827–834.
53. Beelman,C.A. and Parker,R. (1994) Differential effects of translational inhibition in cis and in trans on the decay of the unstable yeast MFA2 mRNA. *J. Biol. Chem.*, **269**, 9687–9692.
54. Shen,W., Liang,X.H. and Crooke,S.T. (2014) Phosphorothioate oligonucleotides can displace NEAT1 RNA and form nuclear paraspeckle-like structures. *Nucleic Acids Res.*, **42**, 8648–8662.
55. Cencic,R., Hall,D.R., Robert,F., Du,Y., Min,J., Li,L., Qui,M., Lewis,I., Kurtkaya,S., Dingledine,R. *et al.* (2011) Reversing chemoresistance by small molecule inhibition of the translation initiation complex eIF4F. *Proc. Nat. Acad. Sci., U.S.A.*, **108**, 1046–1051.
56. Azzam,M.E. and Algranati,I.D. (1973) Mechanism of puromycin action: fate of ribosomes after release of nascent protein chains from polysomes. *Proc. Nat. Acad. Sci., U.S.A.*, **70**, 3866–3869.
57. Wang,L. and Adamo,M.L. (2001) Cyclic adenosine 3′,5′-monophosphate inhibits insulin-like growth factor I gene expression in rat glioma cell lines: evidence for regulation of transcription and messenger ribonucleic acid stability. *Endocrinology*, **142**, 3041–3050.
58. Teixeira,D., Sheth,U., Valencia-Sanchez,M.A., Brengues,M. and Parker,R. (2005) Processing bodies require RNA for assembly and contain nontranslating mRNAs. *RNA*, **11**, 371–382.
59. Parker,R. and Sheth,U. (2007) P bodies and the control of mRNA translation and degradation. *Mol. Cell*, **25**, 635–646.
60. Lima,W.F., De Hoyos,C.L., Liang,X.H. and Crooke,S.T. (2016) RNA cleavage products generated by antisense oligonucleotides and siRNAs are processed by the RNA surveillance machinery. *Nucleic Acids Res.*, **44**, 3351–3363.
61. Thomas,A., Lee,P.J., Dalton,J.E., Nomie,K.J., Stoica,L., Costa-Mattioli,M., Chang,P., Nuzhdin,S., Arbeitman,M.N. and Dierick,H.A. (2012) A versatile method for cell-specific profiling of translated mRNAs in Drosophila. *PLoS One*, **7**, e40276.
62. Tryon,R.C., Pisat,N., Johnson,S.L. and Dougherty,J.D. (2013) Development of translating ribosome affinity purification for zebrafish. *Genesis*, **51**, 187–192.
63. Babendure,J.R., Babendure,J.L., Ding,J.H. and Tsien,R.Y. (2006) Control of mammalian translation by mRNA structure near caps. *RNA*, **12**, 851–861.
64. Boiziau,C., Kurfurst,R., Cazenave,C., Roig,V., Thuong,N.T. and Toulme,J.J. (1991) Inhibition of translation initiation by antisense oligonucleotides via an RNase-H independent mechanism. *Nucleic Acids Res.*, **19**, 1113–1119.
65. Ling,J., Morley,S.J. and Traugh,J.A. (2005) Inhibition of cap-dependent translation via phosphorylation of eIF4G by protein kinase Pak2. *EMBO J.*, **24**, 4094–4105.
66. Liang,X.H., Liu,Q. and Fournier,M.J. (2007) rRNA modifications in an intersubunit bridge of the ribosome strongly affect both ribosome biogenesis and activity. *Mol. Cell*, **28**, 965–977.
67. Xu,Y., Zhang,H.Y., Thormeyer,D., Larsson,O., Du,Q., Elmen,J., Wahlestedt,C. and Liang,Z. (2003) Effective small interfering RNAs and phosphorothioate antisense DNAs have different preferences for target sites in the luciferase mRNAs. *Biochem. Biophys. Res. Commun.*, **306**, 712–717.
68. Schwanhausser,B., Busse,D., Li,N., Dittmar,G., Schuchhardt,J., Wolf,J., Chen,W. and Selbach,M. (2011) Global quantification of mammalian gene expression control. *Nature*, **473**, 337–342.
69. Hutvagner,G. and Simard,M.J. (2008) Argonaute proteins: key players in RNA silencing. *Nat. Rev. Mol. Cell Biol.*, **9**, 22–32.
70. Vickers,T.A., Koo,S., Bennett,C.F., Crooke,S.T., Dean,N.M. and Baker,B.F. (2003) Efficient reduction of target RNAs by small interfering RNA and RNase H-dependent antisense agents. A comparative analysis. *J. Biol. Chem.*, **278**, 7108–7118.
71. Gu,S. and Rossi,J.J. (2005) Uncoupling of RNAi from active translation in mammalian cells. *RNA*, **11**, 38–44.
72. Kennerdell,J.R., Yamaguchi,S. and Carthew,R.W. (2002) RNAi is activated during Drosophila oocyte maturation in a manner dependent on aubergine and spindle-E. *Genes Dev.*, **16**, 1884–1889.